TECHNISCHE UNIVERSITÄT WIEN
Vienna University of Technology

DIPLOMARBEIT

DESIGN AND CONSTRUCTION OF AN ABSORPTION IMAGING SYSTEM FOR BOSE EINSTEIN CONDENSATES

Ausgeführt am Atominstitut
der Technischen Universität Wien

unter der Anleitung von

Univ.Prof. Dipl.-Ing. Dr. Jörg Schmiedmayer
Univ.Ass. Dr.phil. Michael Trupke, MSc.

durch

Michaela Trimmel

Johann-Teufel-Gasse 39-47/4/1, 1230 Wien
mtrimmel@ati.ac.at

Wien, Juli 2011

Abstract

This work describes the design, construction and implementation of a new imaging system for a Rubidium-87 quantum gas experiment. The system consists of two imaging paths: One has a high magnification and the images are collected by a low-noise, high-sensitivity camera for detailed images of the cloud. The other path has a lower magnification and the images are collected by a camera with more modest specifications. This latter path is used for overview images. The desired path is selected by use of a flip mirror. Both paths are used for transversal absorption imaging of the atom cloud. The cloud is in a vacuum chamber controlled by an atom chip. By use of magnetic fields created by wire structures on this chip, the atoms are collected and cooled and can be guided to a fiber detector located at a distance of 5.5 mm from the trapping region. The new imaging system is able to image the cloud throughout trapping, cooling and transport to the detector. The design of the imaging system was constrained by the physical properties of the existing experimental setup. Furthermore, in order to minimize the delivery time only commercial lenses were used. The system design was optimized using the numerical ray-tracing package ZEMAX, and its performance was determined using images of the atom cloud itself. The magnification values were determined using time-of-flight sequences, while the spatial resolution was determined using density ripples in the cloud. This new imaging system has made it possible to image the very dilute atom cloud at the position of the fiber detector, and will thereby enable a thorough characterization of that device.

Zusammenfassung

Der Zweck dieser Arbeit ist das Design, die Errichtung und das Einfügen eines Abbildungssystems in ein Rubidium-87-Gas Experiment zur Betrachtung ultrakalter Atome. Das System besteht aus zwei Abbildungspfaden: Einer besitzt eine hohe Vergrößerung und eine empfindliche Kamera. Dieser Teil bietet detaillierte Aufnahmen der Atomwolke. Der andere Weg hat eine kleinere Vergrößerung und bietet Überblicksbilder aufgenommen durch eine zweite Kamera mit geringer Sensitivität. Zwischen den beiden Pfaden kann mithilfe eines Flip-Spiegels hin und her geschalten werden. Beide Wege dienen der Aufnahme von transversalen Absorptionsbildern einer Atomwolke. Diese Atomwolke befindet sich in einer Vakuumkammer und wird durch einen Atomchip gesteuert. Der Atomchip enthält Drähte, durch die Magnetfelder erzeugt werden, um die Atome zu sammeln, zu kühlen und zum Glasfaserdetektor, welcher am Chip integriert ist, zu transportieren. Das Abbildungssystem ist in der Lage, die Atomwolke während dieser Etappen zu beobachten. Der Platz zum Einbau des Apparats war durch das restliche Experiment beschränkt. Es sollten nur schnell verfügbare Optikelemente verwendet werden. Das Design des Systems wurde durch das 'Ray tracing' Programm ZEMAX gestaltet und optimiert. Die Eigenschaften des fertigen Systems wurden mithilfe der Atomwolke ermittelt. Die Vergrößerung wurde mittels einer Time-of-flight Messung ermittelt, die Auflösung durch sogenannte Density-ripples der Wolke. Das neue Abbildungssystem hat es ermöglicht, sehr dünne Wolken beim Faserdetektor zu sehen und bietet dadurch neue Charakterisierungsmöglichkeiten jenes Detektors.

Acknowledgements

I thank the head of the group, Jörg Schmiedmayer, for the offer of this thesis and the establishment of a group with mutual trust and broad communication opportunities.

I thank my supervisor, Michael Trupke, and the graduate students of the micro-optics-experiment, Dominik Fischer and Wolfgang Rohringer, for all the insights and advise they offered me. Without your support I would have despaired at times. Thanks for enduring my grouching. ☺

Many thanks to all members of the group and the institute for every talk and spent time, regardless of whether at lunch, at coffee breaks, in the hallway, at occasional beers, at professional discussions or not-so professional ones.

I like to take the chance to thank all my fellow students who passed the years of study with me and the folks of the students union in particular. Working and living among you were not only fun but gave also a great deal of possibilities to shape both, the university landscape and myself.

Ich bedanke mich bei meinen Eltern für das tiefe Vertrauen und für jede Unterstützung, die sie mir entgegenbringen. Ich bedanke mich bei meinem Bruder, dafür, dass er mir immer wieder vor Augen führt, dass Wahrheiten oft im Auge des Betrachters liegen; bei meiner Schwester, für die Lebensfreude, die sie ausstrahlt. Ich danke meiner Familie für den Anker den sie bietet.

Ich danke dir, Matthias, dass du mir zur Seite stehst, und dass du mich daran erinnerst, nicht alles zu Ernst zu nehmen.

Contents

1. Introduction

The evolution of ultra cold quantum physics can be followed nicely by investigating the relevant Nobel prizes. Let us have a look at the major parameter, the temperature. The Nobel prize concerning temperature control of atom gases was awarded to Steven Chu, Claude Cohen-Tannoudji and William D. Phillips in 1997 [1, 2, 3]. The challenge in cooling gases is to cool them while keeping a low density so they cannot condense.

In the 1920s Satyendra Nath Bose and Albert Einstein developed a theoretical description of atoms with very low temperature [4]. If a gas of certain atoms is cooled sufficiently, all atoms will condense into the lowest possible energy state. They share the same energy and behave like a single matter wave.

With the right tools in hand, it was only a matter of time for experimentalists to achieve the predicted matter state of Bose-Einstein-condensation (BEC). It was a race won in 2001 by Eric A. Cornell, Wolfgang Ketterle and Carl E. Wieman [5, 6, 7] who were awarded the Nobel prize as the experimental pioneers in Bose-Einstein-condensation. Cornell and Wieman worked together on an experiment using Rubidium atoms. They achieved a temperature of 20 nK. Meanwhile Ketterle used Sodium atoms for his experiments, not only achieving BEC but also making the first interference experiments with two separate BECs. At that time ultra cold atom physics became a widely spread field and is now investigated by research groups all over the world.

The examined atoms are evaporated from a dispenser into a vacuum chamber. Several magnetic fields are necessary to hold the atoms within the desired region as well as to move them to the next location of interest. The experiment in this thesis uses an atom chip to control the cloud of atoms. The atom chip consists of several guiding wires to transport and trap atoms. The trapped atoms are cooled by a combination of laser cooling and evaporative cooling to temperatures below the μK-scale. If the cloud is not yet in the BEC state it is called a 'thermal' cloud. A thermal cloud and a BEC can both be imaged onto a camera by shining laser light onto the atoms. The frequency of the laser is matched to a transition energy of the atoms so they can absorb the light and re-emit the photons in all directions. Then a shadow of the atom cloud can be seen in the propagation direction of the laser light. This shadow can be used to calculate the number and density distribution of the atoms. It is possible to image this ultra cold quantum gas in-situ (within the magnetic trap) or after a time of flight (released atom clouds fall due to gravity and expand).

1.1. Purpose of this work

The aim of this work is the creation of a new imaging system which should enable new experiments due to more detailed pictures of the atom cloud. At the begin of this work, the atom cloud could not be imaged at all regions of the atom chip because the sensitivity of the previous imaging setup was not high enough. An important part of the new system is the new CCD camera with a high quantum efficiency. A ray tracing program will be used for the simulation of the chosen setup. An important factor is the numerical aperture, which is a characteristic value of how much light a system is able to collect. The less light can be gathered from the emitting source, the worse is the result, so, the highest possible numerical aperture is desired. The goal of the new imaging system is a higher resolution and thus a more accurate characterization of the atom cloud. The characteristics of the setup will be determined insitu were it seems sensible (see chapter 8).

1.2. Imaging Techniques

When light is shone onto atoms several effects may occur depending on the wavelength of the light and the transition frequencies of the atom. The passing photons may get absorbed and re-emitted and/or receive a phase shift. These effects are used to gain information about the atom cloud. Depending on which principle is used one speaks of

- 'absorption imaging' when the missing photons from the imaging beam are calculated by comparison of a picture of the imaging beam with atoms and without atoms.
- 'fluorescence imaging' when the spontaneously emitted photons are imaged.
- 'phase contrast imaging' when the phase shift of the photons gets measured.

In this work absorption imaging was used and therefore will be discussed further. Please consult literature for details about the other effects.

1.2.1. Absorption Imaging

When the laser light wavelength is near an atomic transition the light can be absorbed by the atom gas. The excited atom may emit photons into all directions due to spontaneous emission. The absorbed light is missing in the laser beam received by the camera. This shadow image allows conclusions to many attributes of the atomic cloud.

The scattering cross section σ for light absorption of the atom cloud is given by [10]

$$\sigma = h\nu\frac{\Gamma}{2}\frac{1/I_S}{1 + I/I_S + 4\Delta^2/\Gamma^2} \tag{1.1}$$

where I is the intensity of the laser beam, Γ is the natural decay rate and $\Delta = \nu - \nu_0$ is the detuning, with the frequency of the laser light ν and the frequency of the transition

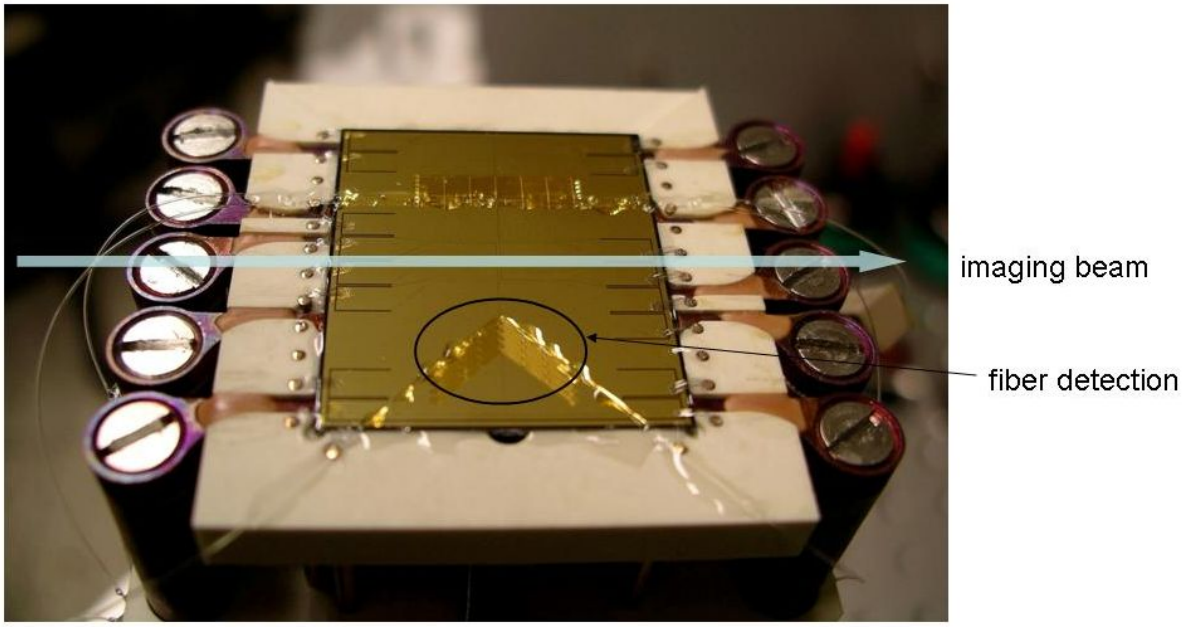

Figure 1.1.: The atom chip. The arrow is indicating the imaging beam. (The fibers on the chip are used for integrated optics which are carried out in [8, 9] and are not discussed in this thesis.)

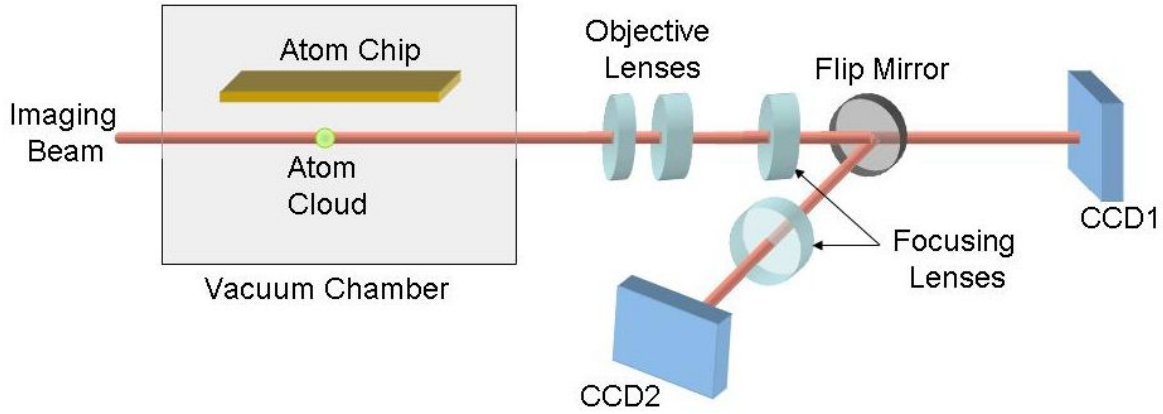

Figure 1.2.: The concept of the imaging system is that there are two arms, one for high resolution close up pictures with one camera, the second arm for overview pictures received by the other CCD. The desired path can be selected with the help of a flip mirror.

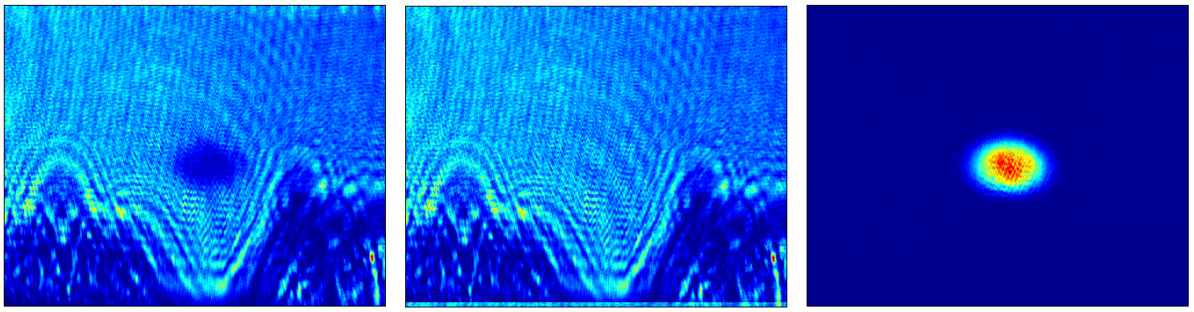

Figure 1.3.: To gain an absorption image two pictures have to be taken: the first picture is an image of the shadow of the atom cloud; the second picture shows the intensity without any atoms. The structures seen on the pictures are bond wires of the atom chip. According to equation 1.4, the first image corresponds to $I - I_B$ and the second to $I_0 - I_B$. The absorption image is a result from the first two pictures and can be seen in the third.

ν_0. The saturation intensity I_S for the transition of a two-level system is given by $I_S = \frac{\hbar\omega^3\Gamma}{12\pi c^2}$. The cross section can be written using $\lambda = 2\pi c/\omega$ and the on-resonance cross section $\sigma_0 = \frac{\hbar\omega\Gamma}{2I_S} = \frac{3\lambda^2}{2\pi}$, so that

$$\sigma = \frac{\sigma_0}{1 + I/I_S + 4\Delta^2/\Gamma^2}. \tag{1.2}$$

The decrease of the intensity of the beam shone on the atom gas depends on the cross section and on the number density n of the cloud. For $I \ll I_S$ it is described by the Beer-Lambert law

$$I = I_0 \exp\left(-\sigma \int_{z_{min}}^{z_{max}} n(x, y, z)\, dz\right) \tag{1.3}$$

with the incident beam intensity I_0 and the propagation direction of the light z, $|z_{max} - z_{min}|$ is the extent of the cloud along the propagation axis. The local density of the atom cloud $n(x, y, z)$ can be used to define the column density or line density $\tilde{n}$ by integration along the direction of the light (z-axis) $\tilde{n}(x, y) = \int n(x, y, z')\, dz'$. However, the observable of the system is the optical density or optical depth $OD = -\sigma \int_{z_{min}}^{z_{max}} n(x, y, z')\, dz'$ and can be calculated via the intensities, $OD = -\ln(I/I_0)$.

I_0 and I can be easily achieved in the experiment. I_0 corresponds to the image taken without atoms (only the laser beam) and I is obtained by taking an image with atoms. Usually, thermal noise or background light are present and these intensities have to be background corrected. For this reason a third picture is taken without atoms and without laser light. The corresponding intensity I_B is subtracted from both intensities. The optical depth then reads

$$OD = -\ln \frac{I - I_B}{I_0 - I_B} \tag{1.4}$$

The scattering rate R of an atom offers a calculation for the atom number [11]. The number of photons scattered per second is given by NR where N is the number of atoms

in a volume dx^3 and

$$R = \frac{2\pi\Gamma}{2}\frac{I/I_S}{1 + I/I_S + 4\Delta^2/\Gamma^2} = \frac{2\pi I}{h\nu}\sigma \tag{1.5}$$

with the laser frequency ν. For the intensity I the incoming flux through an area A is $\frac{AI}{h\nu}$ and the exiting flux $\frac{A(I-dI)}{h\nu}$. Consequently, another expression for the scattered photons can be written as

$$\frac{AI}{h\nu} - \frac{A(I - dI)}{h\nu} = -\frac{AdI}{h\nu} = NR \tag{1.6}$$

Transversal Imaging The atom sample is a cigar shaped gas cloud. The elongated direction of the cloud is the one commonly imaged. The imaging beam propagates through the cloud where it is slender. This is called transversal imaging.

1.3. Off resonance: Lensing Effect

If the laser light is not on resonance with the atomic transition the traversing photons gain a phase shift. If the light is blue-detuned ($\Delta > 0$) the atom cloud acts as diverging lens, if it is red-detuned ($\Delta < 0$) the cloud acts as converging lens. This effect is caused by the refractive index of the atoms and is often called lensing effect. Normally, these refraction effects of the atoms are avoided for absorption imaging. But it can be used for focusing the imaging system (see section 8.1.1). The cloud shape changes if the imaging beam is detuned (see fig. 3.2). From the shape of the cloud and knowledge about the detuning one can say if the imaging system is inside focus or outside focus. If the cloud shape looks the same for blue- and for red-detuned light, the system is in focus. In fact, this focusing approach works better using condensates instead of thermal clouds because condensates have a smaller extent, so a higher optical density and are less affected by the magnetic trap.

When the imaging laser is detuned from the atom transition wavelength the atom cloud becomes less absorptive. If the cloud is also defocused, the intensity profile changes due to diffraction and scattering effects. For a given detuning there are in focus and out of focus characteristics which are exactly opposite if the detuning changes its sign with respect to the atom transition. The phenomenological description can be found in [12] and a picture of the effect is shown in figure 1.4.

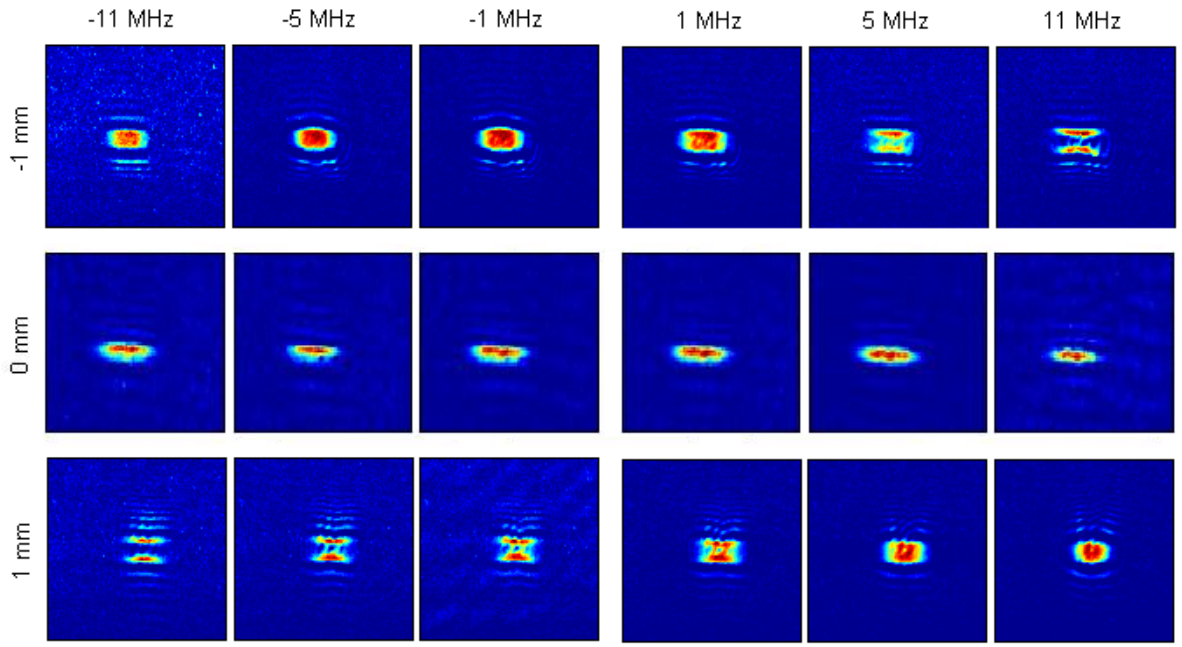

Figure 1.4.: Detuning Scan for different defocus values. Rows are different detunings from the atomic transition, vertical are different defoci. The shape of the cloud changes for different defocus values while the detuning stays the same and for different detunings when the defocus is kept untouched. The behavior of the cloud is mirrored at no detuning (0 MHz). The focus can be found by searching the position where red detuning (negative MHz values) and blue detuning (positive MHz values) leads to the same cloud shape.

2. Geometric Optics

Our system can be explained and calculated in terms of geometric optics. It's an approximation which is appropriate in cases when a light beam has a diameter far bigger than the wavelength, so that diffraction effects can be neglected. Reflection is then given by $sin\alpha = sin\alpha'$, and refraction according to Snell's law by $\frac{sin\alpha}{sin\beta} = \frac{n_2}{n_1}$, see figure 2.1. As geometric optics cannot account for diffraction, this will be discussed separately in sec. 3.

2.1. Thin Lens

The approximation of a thin lens can be used if the maximum distance of the lens surfaces is small compared to the focal length. The refraction of the two lens surfaces can be substituted by a refraction on the plane in the middle of the lens. With the definition of the curvature of a lens surface as in figure 2.2 the lens equation of a thin lens can be written as

$$\frac{1}{a} + \frac{1}{b} = (n_2 - n_1)(\frac{1}{R_1} - \frac{1}{R_2}) \tag{2.1}$$

where a is the object distance, b the imaging distance R_1 the curvature of the first lens surface, R_2 the curvature of the second lens surface, n_2 is the refraction index of the lens and n_1 the refraction index of the surrounding medium. Usually, the surrounding material is vacuum or air. So we set $n_1 = 1$ and $n_2 = n$ for the next equations. For an explanation of the used parameters please see also figure 2.2.

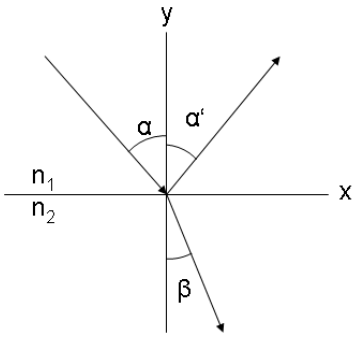

Figure 2.1.: Reflection and refraction on a surface. The arrows indicate the direction of the light propagation.

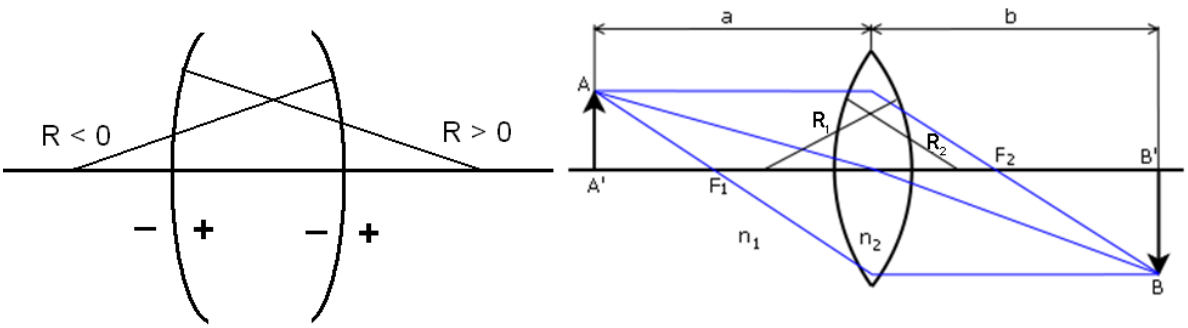

Figure 2.2.: left: Definition of the sign of the radius of curvature of a lens surface. right: Parameters for the thin lens equation, see eq. (2.1)-(2.3) .

The focal length of the thin lens is given by $f = \frac{1}{n-1}(\frac{R_1 R_2}{R_2 - R_1})$. The imaging equation for such a system reads

$$\frac{1}{a} + \frac{1}{b} = \frac{1}{f}. \tag{2.2}$$

The magnification[1] of the lens is given by

$$M = \frac{\overline{BB'}}{\overline{AA'}} = -\frac{b}{a} = \frac{f}{f-a}. \tag{2.3}$$

2.2. Notations

This section will explain some basic expressions used in geometric optics and can be skipped when you are already familiar with these basics.

- **Pupils and Stops**

The **aperture stop** is the element of the system which is responsible for how many light reaches the image plane. For example, it can be a lens or a supplementary aperture.
The **field stop** defines the field of view by limiting the size of the object that can be imaged. It is often the case that the detector size limits the field of view.
The **entrance pupil** is the (virtual) image of the aperture stop seen from the position of the object. If there is no lens before the aperture, the entrance pupil and the aperture stop are the same. Otherwise the entrance pupil is magnified or demagnified and dislocated to the aperture stop.
The **exit pupil** is the corresponding value to the entrance pupil. It's the aperture stop seen from the image plane.

[1] Negative sign means that the image is upside down.

Lens properties: *AC-254-200-B*, focal length: 200.315 mm

	Curvature	Thickness	Diameter	Glass
Surface 1	106.41	4	25.4	LAKN22
Surface 2	-96.61	4	25.4	SF10
Surface 3	2000	-	25.4	-

Lens properties: *AC-508-400-B*, focal length: 397.006 mm

	Curvature	Thickness	Diameter	Glass
Surface 1	280.55	4.5	25.4	LAKN22
Surface 2	-208	2.6	25.4	SFL6
Surface 3	-859	-	25.4	-

Lens properties: *AC-508-1000-A1*, focal length: 1000 mm

	Curvature	Thickness	Diameter	Glass
Surface 1	738.5	4	50.8	BK7
Surface 2	-398.1	2	50.8	SF2
Surface 3	-1023.3	-	50.8	-

Table 2.1.: *All units in mm.* Lens properties according to the manufacturer (Thorlabs): Lens type-diameter-focal length-coating. The column 'Curvature' gives the radii of curvature. All used lenses are achromats, their properties are listed in table 2.2.

- **Rays**

A **ray** is the direction of propagation of a light wave, in other words the normal to the phase front of the wave.
Meridional rays are rays in the plane of the optical axis. If z is the optical axis and y perpendicular to it, than a meridional ray is limited to the y-z-plane.
Nonmeridional rays are also called **skew rays** and do not intersect the optical axis.
Marginal rays have their origin on the optical axis at the object point and go to the edge of the entrance pupil.
Chief rays are the complement to the marginal rays. A chief ray starts at an off-axis object point. They cross the entrance pupil at its center.

2.3. Aberrations

Geometric optics is based on idealized conditions. A real system will show a different behavior. These deviations are called aberrations. One can think of two different types of aberrations. The first type are aberrations caused by dispersion. This effect has its origin in the wavelength-dependent refraction index $n(\lambda)$. It's the same effect which causes the spread of daylight into different wavelengths while passing a prism. We call these aberrations *chromatic aberrations*. The counterpart are *monochromatic aberrations*. They are due to rays hitting the optical features at different heights or at different angles and propagate differently because of it.

2.3.1. Seidel Aberrations

Famous expressions dealing with aberrations are the Seidel aberrations. They are named after the mathematician Philipp Ludwig von Seidel (1821-1896) who decomposed the monochromatic aberrations into five parts: spherical aberration, coma, astigmatism, field curvature and distortion. The aberrations will be explained later on.
Paraxial optics takes only rays in a narrow region about the optical axis into account. The approximation made is that $\sin\phi = \phi$ and $\cos\phi = 1$ where ϕ is the angle between the ray and the optical axis. The Taylor expansion of the trigonometric functions are

$$\sin\phi = \phi - \frac{\phi^3}{3!} + \frac{\phi^5}{5!} - \frac{\phi^7}{7!} + ...$$

$$\cos\phi = 1 - \frac{\phi^2}{2!} + \frac{\phi^4}{4!} - \frac{\phi^6}{6!} + ...$$

The approximation of the paraxial optics is improved by the Seidel aberrations which uses the first two terms of the expansions. The Seidel aberrations are therefore also called the third-order-aberrations.

2.3.2. Wavefront Description

Being x and y the exit pupil coordinates and x_0, y_0 the coordinates of the image point, the wavefront can be written in an expression depending on these coordinates. Based on the assumption of spherical symmetry of the imaging system, there are no changes if there is a rotation about the z (propagation) axis. We then can choose the image point to be on a plane containing the x and z axes, hence choose y_0 to be zero. The wavefront W can than be described as [13]

$$\begin{aligned} W(x,y,x_0) =& a_1(x^2+y^2) + a_2 x x_0 + a_3 x_0^2 \\ &+ b_1(x^2+y^2)^2 + b_2 x x_0 (x^2+y^2) + b_3 x^2 x_0^2 \\ &+ b_4 x_0^2 (x^2+y^2) + b_5 x x_0^3 + b_6 x_0^4 + ... \end{aligned} \tag{2.4}$$

The first term corresponds to defocus (decenter in longitudinal direction), the second to a tilt (decenter in transversal direction) and the third term to a phase shift. The coefficients of these terms (a_1, a_2, a_3) are set to zero. For a discussion of the terms with coefficients b_1 to b_6 we change to polar coordinates. With $x = \rho\cos\theta$ and $y = \rho\sin\theta$ the wavefront transforms into

$$\begin{aligned} W(x_0,\rho,\theta) =& \frac{1}{8} S_1 \rho^4 + \frac{1}{2} S_2 x_0 \rho^3 \cos\theta + \frac{1}{2} S_3 x_0^2 \rho^2 \cos^2\theta \\ &+ \frac{1}{4}(S_3 + S_4) x_0^2 \rho^2 + \frac{1}{2} S_5 x_0^3 \rho \cos\theta + ... \end{aligned} \tag{2.5}$$

The coefficients S_1 to S_5 are the Seidel coefficients. Every term now corresponds to a specific type of aberration. The corresponding aberrations are: spherical aberration, coma, astigmatism, field curvature and distortion. An explanation of these aberrations can be found in appendix A.

2.3.3. Achromats

Conventional lenses have different refraction indices for different wavelengths, also called chromatic aberration. Although we use monochromatic laser light, achromats enhance the imaging performance. With the right choice of glasses spherical aberration and coma can be improved as well. For common glass the refractive index increases for decreasing wavelengths. This means for a biconvex lens that blue light is focused closer to the lens than red light. To compensate this dispersion effect Chester Moor Hall invented the achromat in 1733, an idea that gets published and patented years later in 1758 by John Dollond. Achromats are compounds of two thin lenses: A convex lens with a small dispersion (crown) and a concave lens with a high dispersion (flint). A lens is 'achromatized' for $\lambda 1$ and $\lambda 2$ if the focus lengths of the wavelengths overlap.

All of the achromats used in the setup are called Fraunhofer cemented[2]. In such a type of achromat the two lenses are tight connected, the lens shapes are double-convex

[2]There are also other types of achromat designs which are listed in [14]: Hecht, Optics: Chromatic Aberrations.

	Glass Name	Refractive Index n_d	Abbe Number V_d
Achromat 1	LAKN22	1.6511	55.89
	SF10	1.7283	28.41
Achromat 2	LAKN22	1.6511	55.89
	SFL6	1.8052	25.39
Achromat 3	BK7	1.5168	64.17
	SF2	1.6477	33.85

Table 2.2.: Glass overview of the used achromats. K stands for crowns and F for flints. The other letters as the numbers specify the glass type. The LAKN22, for example, is a lanthanum crown and a rare-earth glass, which results in the low dispersion (high Abbe number).

for the crown and concave-nearly-planar for the flint. The combined shape is convex-nearly-planar [14, 15].

Glasses for achromats are characterized by their refractive index and their Abbe number. The Abbe number V_d calculates $V_d = \frac{n_d - 1}{n_F - n_C}$ where the subscript d relates to the yellow line in the Helium spectrum (587.56 nm); n_F and n_C are the refractive indices of the blue and red line from the Hydrogen spectrum (486.13 nm and 656.28 nm, respectively). Glasses with $n_d > 1.60, V_d > 50$ and $n_d < 1.60, V_d > 55$ are crowns, the others flints, see table 2.2 and figure 2.3.

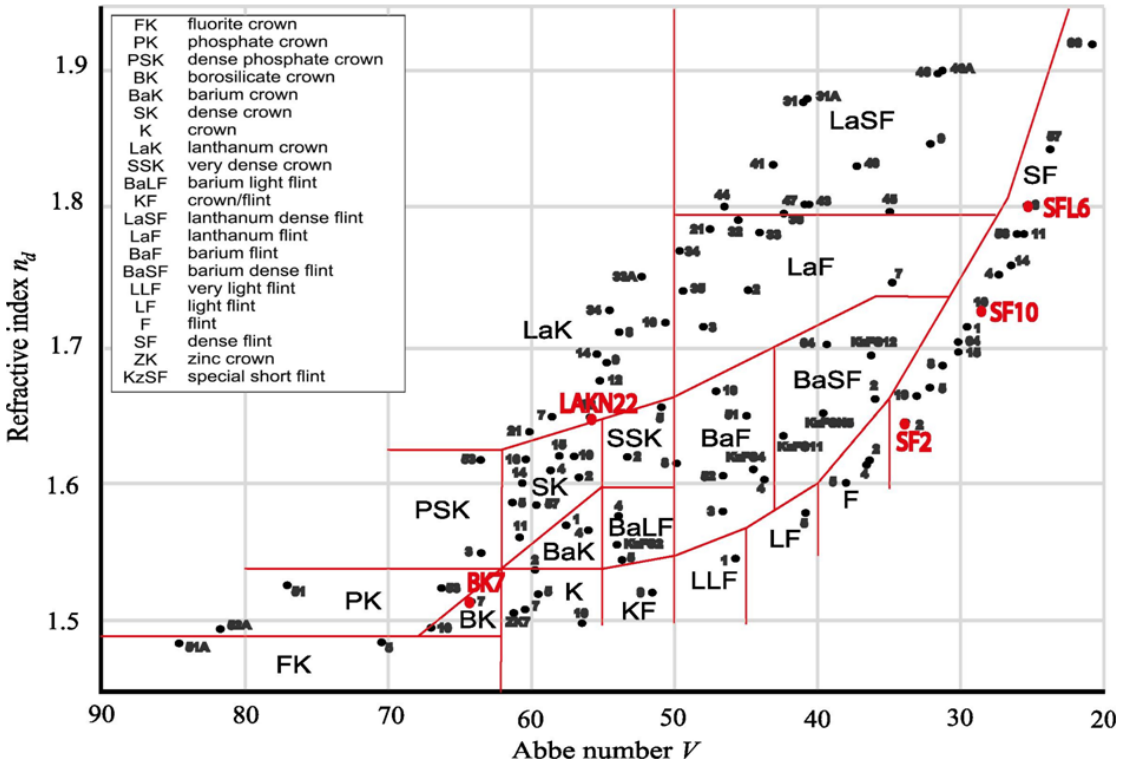

Figure 2.3.: Glass map. The used glasses are highlighted.

3. Diffraction

Diffraction occurs when a wave is obstructed by any kind of obstacle (transparent or opaque). There are regions where the amplitude or phase of the wavefront are altered. The different wavefronts interfere behind the obstacle. The diffraction pattern is the outcoming energy-distribution of the effect [14, 15].

We assume that we have a plane (x, y) at $z = 0$ where we find a screen with an opening σ. The field amplitude on this plane is $E_S(x, y) = E_0(x, y)e^{i\phi(x,y)}$ with $\phi = \omega t - kR$ if the light source is a point source at $(0, 0, -g)$. Then the field amplitude on a plane (x', y') at $z = z_0$ can be given by $E_P = \int\int CE_S \frac{e^{-ikr}}{r} dxdy$[1] where $dxdy = d\sigma$ corresponds to the surface of the opening σ and $C = \frac{i\cos\theta}{\lambda}$. The resulting field in the plane (x', y', z_0) depends on the distance between the screen and the plane.

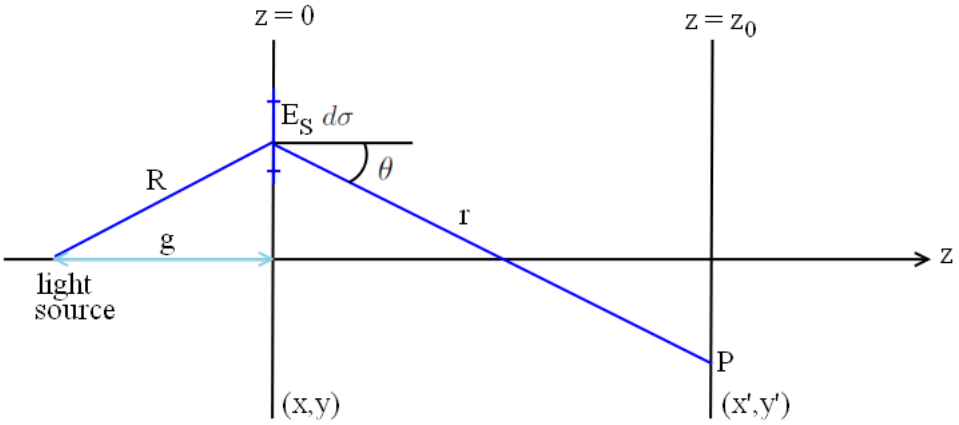

- **Near field**

Using the Taylor evolution r can be approximated as

$$r = \sqrt{z_0^2 + (x - x')^2 + (y - y')^2} \approx z_0 \left(1 + \frac{(x - x')^2}{2z_0^2} + \frac{(y - y')^2}{2z_0^2} + ...\right) \tag{3.1}$$

Furthermore is $x/z_0 \ll 1$ and $y/z_0 \ll 1$ if the distance between screen $(x, y, 0)$ and plane (x', y', z_0) is bigger than the values x and y. Then $\cos\theta = z_0/r \approx 1$.

This assumptions give the near field or *Fresnel approximation*:

$$E(x', y', z_0) = i\frac{e^{-ikz_0}}{\lambda z_0} \int_{-\infty}^{\infty}\int_{-\infty}^{\infty} E_S(x, y) \exp\left[\frac{-ik}{2z_0}\left((x - x')^2 + (y - y')^2\right)\right] dxdy \tag{3.2}$$

[1] This is the Fresnel-Kirchhoff diffraction integral. For details see the textbook of your choice, for example, [15].

- **Far field**

The x^2 and y^2 terms in equation 3.1 can be neglected if $z_0 >> \frac{(x^2+y^2)}{\lambda}$.

$$r \approx z_0 \left(1 - \frac{xx'}{z_0^2} - \frac{yy'}{z_0^2} + \frac{x'^2 + y'^2}{2z_0^2}\right) \tag{3.3}$$

This approximation is the far field or *Fraunhofer diffraction* and yields

$$\begin{aligned} E(x', y', z_0) =& i\frac{e^{-ikz_0}}{\lambda z_0} \exp\left[\frac{-i\pi(x'^2 + y'^2)}{\lambda z}\right] \\ & \cdot \int_{-\infty}^{\infty}\int_{-\infty}^{\infty} E_S(x, y) \exp\left[\frac{ik}{z_0}(x'x + y'y)\right] dxdy \end{aligned} \tag{3.4}$$

3.1. The rectangular aperture

The limiting aperture in our setup is given by to coils. They limit on the left and right handside leaving bottom and top open. It isn't a circular aperture and can most likely be described by a wide single slit.

When a monochromatic plane wave propagating in the z-direction reaches an aperture the diffraction effects in the far-field approximation are [14]:

$$dE = \frac{\epsilon_A}{r} e^{i(\omega t - kr)} dS \tag{3.5}$$

where dS is the differential area within the aperture, ϵ_A is the source strength per unit area and dE is the optical disturbance at an arbitrary point P, r is the distance vector between dS and P. When the aperture is in the (x, y)-plane and the coordinates of P are (X, Y, Z), the total disturbance E according to the Huygens-Fresnel principle at P is

$$E = \frac{\epsilon_A e^{i(\omega t - kR)}}{R} \int\int_{Aperture} e^{ik(xX+yY)/R} dS \tag{3.6}$$

where R is the distance of the center of the aperture to the point P. If the aperture has the shape of a rectangle with edge lengths a and b, the total disturbance can be written as

$$E = \frac{\epsilon_A e^{i(\omega t - kR)}}{R} \int_{-a/2}^{a/2} e^{ekxX/R} dx \int_{-b/2}^{b/2} e^{ikyY/R} dy \tag{3.7}$$

where $dS = dxdy$. Evaluation of the integrals leads to

$$E = \frac{A\epsilon_A e^{i(\omega t - kR)}}{R} \frac{\sin\alpha}{\alpha} \frac{\sin\beta}{\beta} \tag{3.8}$$

where $\alpha = kaX/2R$ and $\beta = kbY/2R$ and A is the area of the aperture.

The irradiance I can than be written as

$$I(X, Y) = \langle(\mathrm{Re}\, E)^2\rangle = I(0) \left(\frac{\sin\alpha}{\alpha}^2\right) \left(\frac{\sin\beta}{\beta}^2\right) \tag{3.9}$$

The irradiance pattern depends inversely on the aperture dimensions. A horizontal opening will produce a vertical pattern.

The single slit In the case of a single slit with a width of b and a length of l the optical disturbance at the point P is given by

$$dE = \frac{\epsilon_L}{R} \sin(\omega t - kr) dx \tag{3.10}$$

$$\begin{aligned} E &= \frac{\epsilon_L}{R} \int_{-b/2}^{b/2} \sin(\omega t - k(R - x \sin\theta)) dx \\ &= \frac{\epsilon_L b}{R} \frac{\sin\beta}{\beta} \sin(\omega t - kR) \end{aligned} \tag{3.11}$$

with $\beta = \sin\theta(kb/2)$ where θ is the angle between the center of the aperture (which is chosen to lie on the z-axis) and the point P. The irradiance I is

$$I(\theta) = I(0) \left(\frac{\sin\beta}{\beta} \right)^2 \tag{3.12}$$

3.2. The impact of the chip

The laser beam runs parallel to the chip surface. If the beam clashes the chip diffraction effects follow. To prevent that from happening the cloud should be at some distance from the chip surface. This means a certain time of flight. 1.2 mm are found to be a minimum distance for ideal pictures, see fig. 3.1. This corresponds to a time of flight of 15 ms.

3.3. Mathematical description of the lensing effect

Following up the brief description in section 1.3 the lensing effect can be described mathematically. Details of the calculation and considerations made in the following formulas, can be found in [16, 17].

We start with a plane wave $f(\mathbf{x}) = f_0 exp(-\mu(\mathbf{x}) + i\phi(\mathbf{x}))$ where $\mu(\mathbf{x}) = k\beta\rho(\mathbf{x})$ is the absorption with coefficient β and $\phi(\mathbf{x}) = k\delta\rho(\mathbf{x})$ is the phase shift with coefficient δ, $k = 2\pi/\lambda$ and $\rho(\mathbf{x})$ is the column density along the optical path. Using a Fresnel approximation[2] and $I = |f|^2$, the Fourier transform of the diffracted intensity at z can be written as $\mathcal{F}[I(\mathbf{x}, z)] = I_0(\delta(\mathbf{u}) - 2\cos(\pi\lambda z u^2)\mathcal{F}[\mu(\mathbf{x})] + 2\sin(\pi\lambda z u^2)\mathcal{F}[\phi(\mathbf{x})])$, where $\mathbf{u}$ is the spatial frequency conjugate to $\mathbf{x}$ and weak absorption[3] as weak phase shift[4] are implied. The Fourier transform of the normalized contrast can be written depending on the column density: $\mathcal{F}[(I - I_0)/I_0] = 2k(\delta\sin(\pi\lambda z u^2) - \beta\cos(\pi\lambda z u^2))\mathcal{F}[\rho(\mathbf{x})]$. This

[2] $f(\mathbf{x}, z) = \int_{-\infty}^{\infty} f(\mathbf{x}) exp(\frac{i\pi}{\lambda z}|\mathbf{x} - \mathbf{x}'|^2) d\mathbf{x}'$

[3] $2\mu(\mathbf{x}) \ll 1$

[4] $|\phi(\mathbf{x} + \lambda z\mathbf{u}/2) - \phi(\mathbf{x} - \lambda z\mathbf{u}/2)| \ll 1$; $|\phi(\mathbf{x})| \ll 1$ would be sufficient as well

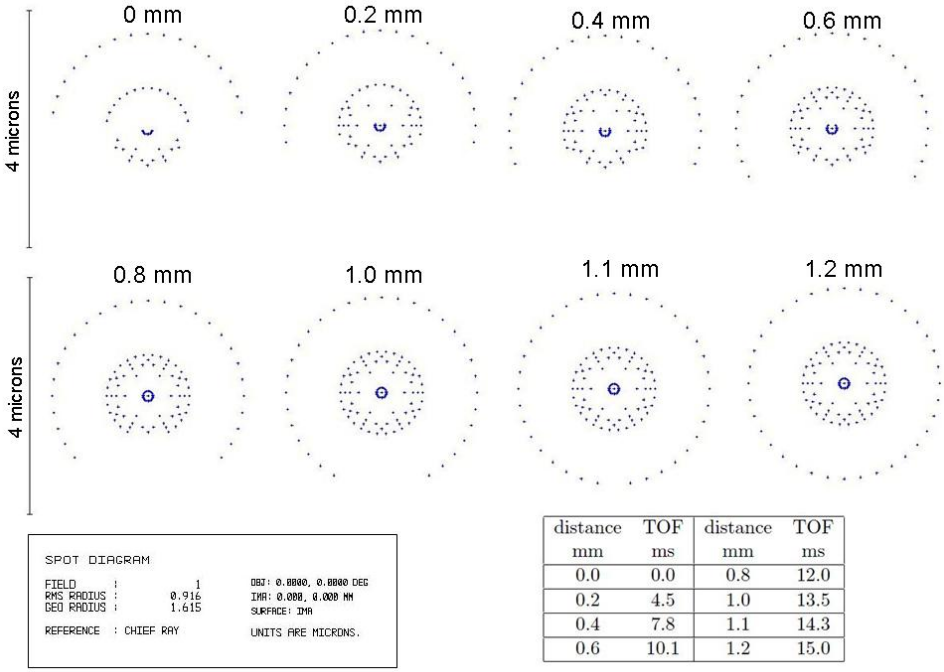

distance mm	TOF ms	distance mm	TOF ms
0.0	0.0	0.8	12.0
0.2	4.5	1.0	13.5
0.4	7.8	1.1	14.3
0.6	10.1	1.2	15.0

Figure 3.1.: If the TOF is short the atom chip may cause diffraction. We see spot diagrams (see sec. 6.2) for different time of flights. The distance is the distance from the chip surface to the optical axis. 0 mm means that half space is covered by the chip. The ideal image is reached at 1.2 mm. The conversion to TOF takes the length between chip surface and center of the insitu cloud ($\sim 100\mu m$) into account.

formula can be rewritten in terms of cold atoms with closed transition (which is used in the graphs in figure 3.2):

$$\begin{aligned}\mathcal{F}\left[\frac{I-I_0}{I}\right] &= \frac{\sigma_0}{1+4\Delta^2}[2\Delta\sin(\pi\lambda z u^2)+\cos(\pi\lambda z u^2)]\mathcal{F}[\rho(\mathbf{x})] \\ &= -2kh(u,z)\mathcal{F}[\rho(\mathbf{x})]\end{aligned} \tag{3.13}$$

where the refraction index n was used

$$n = 1 + N(\mathbf{r})(\delta + i\beta) = 1 + N(\mathbf{r})\frac{\sigma_0\lambda}{4\pi}\frac{i-2\Delta}{1+4\Delta^2} \tag{3.14}$$

with the number density of atoms N, detuning Δ in natural linewidths, resonant cross section σ_0; z is the defocus and $h(u,z)$ is the contrast transfer function.

When a detuned and/or defocused picture is taken, the initial column density can by retrieved by

$$\rho(\mathbf{x}) = \frac{1}{2k}\mathcal{F}^{-1}\left[\frac{h(u,z)}{h(u,z)+\alpha^2}\mathcal{F}\left[\frac{I-I_0}{I}\right]\right] \tag{3.15}$$

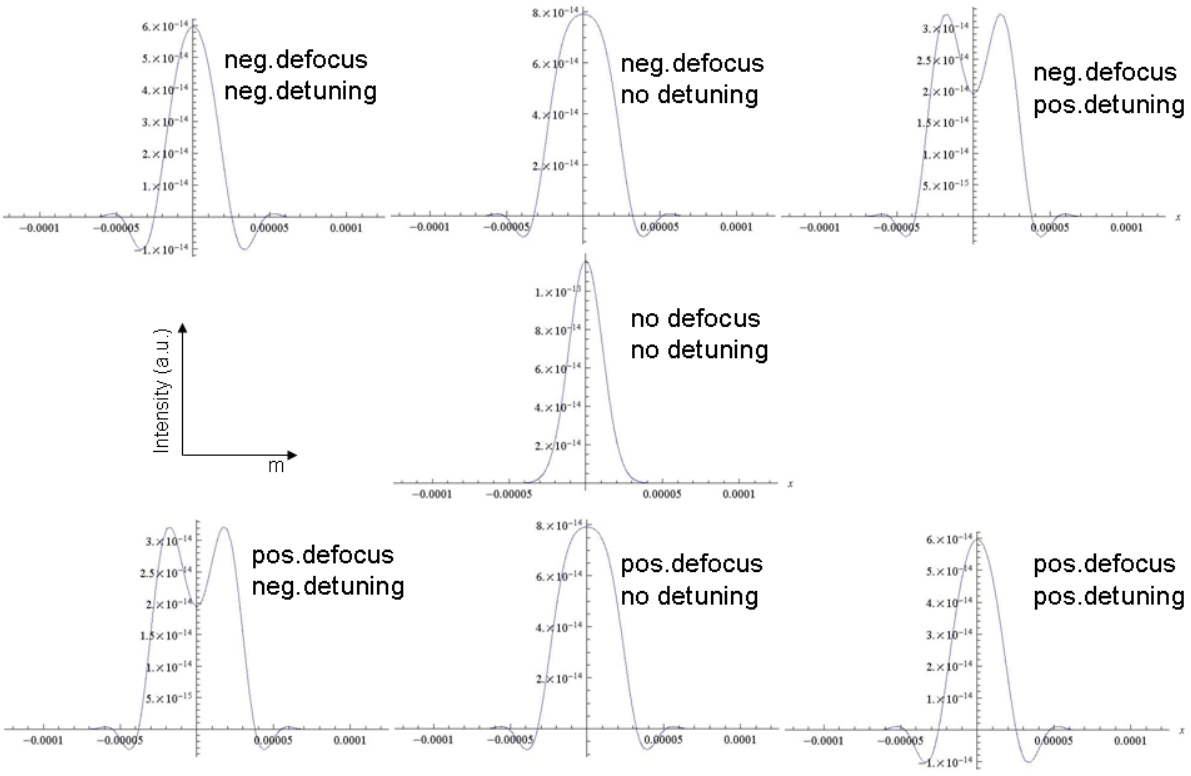

Figure 3.2.: Simulation of the behavior of an atom cloud undergoing different defoci and different detunings using equation 3.13. When an image is defocused it is not possible to know if the picture is inside focus or outside focus without the help of a detuned laser beam. Once the laser beam is detuned the cloud shape behaves different for red and blue detunings whereby the attitude are complementary to the different defocus signs. This figure can qualitatively explain the clouds in figure 1.4 on page 6 and gives rise to a focusing method as discussed in section 8.1.1.

with Tikhonov parameter α [18].

4. Fourier Optics

The progression from an amplitude function at the entrance of the system to the amplitude function at the exit of the system is described by the transfer function. The development from a delta-function is called the point spread function of the system. In other words the point spread function describes the system's response to a point source at the image plane.

4.1. Point Spread Function

When $dxdy$ is the source element on the object plane, the irradiance on the image plane dI_i at a point (X, Y) is given by

$$dI_i(X, Y) = S(x, y; X, Y)I_0(x, y)dxdy \tag{4.1}$$

where $Sdxdy$ is the profile of the irradiance distribution on the image plane. $S(x, y; X, Y)$ is called the point spread function.

If the object is a point source and the system is ideal the point spread function is given by the Airy irradiance distribution

$$I(\theta) = I(0)\left(\frac{2J_1(ka\sin\theta)}{ka\sin\theta}\right)^2 \tag{4.2}$$

with the first order Bessel function J_1.

The central maximum is called Airy disc, ∼84 % of the light lies within this disc. The radius q of the Airy disc is determined by the first dark ring of the Bessel function $J_1(x_1) = 0$. Wich is fulfilled at $x_1 = 3.83$, in our case $x_1 = ka\sin\Theta = \frac{kaq}{R}$. The radius is than given by $q = 3.83\frac{R}{ka}$. With $k = \frac{2\pi}{\lambda}$ and for a lens focused on the image plane $R \approx f$ and $2a = D$ with the focal length f and the aperture diameter D. The Airy disc diameter then is

$$q \approx 1.22\frac{f\lambda}{D} \tag{4.3}$$

4.2. Transfer Functions

The quality of an optical system can be evaluated by the limit of resolution. The greater the resolution the better is the optical system as it means that the system is able to reproduce more details. Transfer functions give insight into the image formation.[14, 19]

A resolution target consisting of a harmonic grating of light and dark rectangular bars can be used for determining the resolution limit. The bars are equidistant and

get narrower and narrower. One sequence cycle is called a line pair. The alternating lines correspond to a spatial frequency and are often expressed as in terms of line pairs per mm. An imaging system transmits low spatial frequencies for coarse changes in the object and it transmits high spatial frequencies for details of the objects. A limit will be reached where the 'black' and 'white' lines will no longer be distinguishable. This is the resolution limit. To put it another way, the system has a cutoff spatial frequency where no further details may be imaged. Hence an optical system is a low pass filter. One can say that the system transfers the different harmonic components with different efficiency. That's why we consider Fourier analysis for determining imaging performance.

4.2.1. Optical Transfer Function OTF

An object source is considered to be plane waves traveling through the system. A question is, how does the system alter the phase or amplitude of these waves. As the object is composed of Fourier components the harmonic constituents are transformed by the optical system. A function that describes this process is the optical transfer function. The OTF is complex and depends on the spatial frequency. It consists of a modulus called modulation transfer function and a phase called phase transfer function. The phase transfer function PTF (not to be mistaken for the point spread function PSF) gives the relative phase shift and is of less interest here. Not so the modulation transfer function which we will give a closer look.

4.2.2. Modulation Transfer Function MTF

The MTF is widely used for determining the system's performance and gives the contrast of the gained image as a function of the spatial frequency. The MTF is the function over all spatial frequency of the image modulation over the object modulation. Where the function hits the abscissa there is the cutoff frequency. In principle the overall MTF of an imaging system is the product of the independent MTFs of the used components (if known). But this principle does not hold for consecutive lenses as the aberration of one lens may compensate for aberrations of another.

If the system is diffraction limited the cutoff depends only on the size of the aperture. The system depends only on diffraction. The higher the spatial frequency k the higher the angle Θ of the imaging system has to become that k can by imaged. The maximum angle α of the system is limited by the numerical aperture. α gives the cutoff frequency $k_0 = \frac{\alpha}{\lambda}$ where λ is the wavelength of the used laser light [19].

An evaluation of the MTF of the final imaging system can be found in section 8.3 on page 50.

4.3. Diffraction limit and Rayleigh criterion

Assuming the lenses in an optical setup have no aberrations the image still will not be perfect. The object scatters the incoming light waves and is responsible for interferences

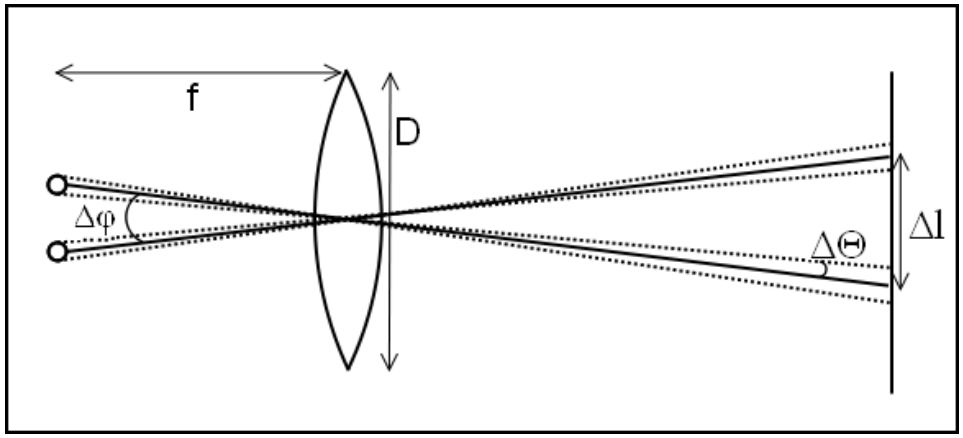

Figure 4.1.: Parameters of the Rayleigh criterion. See equation 4.4.

between the waves. The absolute limit of the image quality is given by these diffraction effects. A point source creates an Airy disk (see sec. 4.1) with radius $q = 1.22\frac{f\lambda}{D}$ or written in radians $\frac{q}{f} = \sin\Delta\Theta \approx \Delta\Theta = 1.22\frac{\lambda}{D}$, where $\Delta\Theta$ is the angular half width of the resulting image point, f the focal length of the lens, λ the wavelength of the image beam and D the aperture diameter. Two point sources can easily be resolved if their angular distance $\Delta\phi$ is much larger than the angular half width of the single image points. When the distance decreases, a value will be reached at which the two points cannot be resolved as individual objects any more but as one object of bigger size. Rayleigh offered a criterion for the minimum distance two point sources must have, so they are resolvable as individuals. This criterion states that the nearest possible still resolvable position of two object points is reached if the center of one Airy disk overlaps with the first minimum of the Airy pattern of the other source. In terms of angular separation this yields

$$\Delta\phi_{min} = 1.22\frac{\lambda}{D} \tag{4.4}$$

Or in terms of center-to-center separation of two Airy patterns on the image plane, where Δl_{min} is called resolution limit

$$\Delta l_{min} = 1.22\frac{f\lambda}{D} \tag{4.5}$$

An optical system is called to be **diffraction limited** if the aberrations of it are smaller than the resolution limit given by Rayleigh's criterion. This is the case if the spot size on the image plane is smaller than the Airy disk.

The diffraction limited resolution of our system is ca. 5.2 μm[1].

[1] $1.22\frac{\lambda f}{D}$ for $\lambda = 780nm$, distance atom cloud to aperture $f = 137mm$, diameter aperture $D = 25mm$.

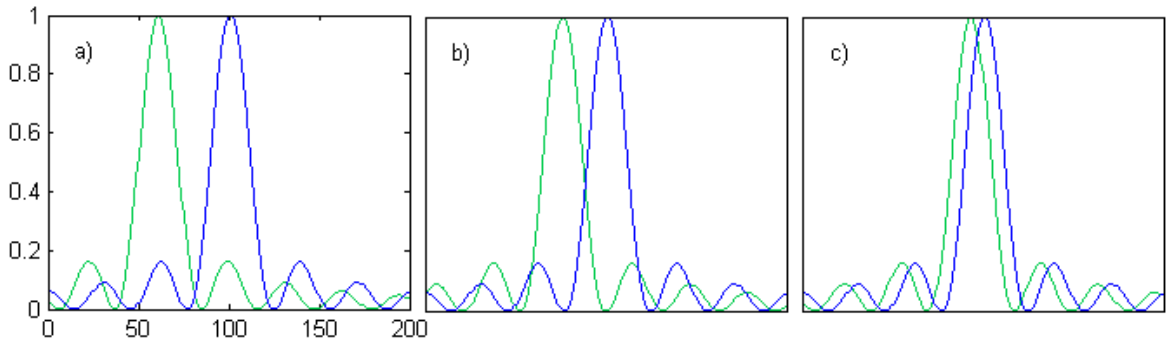

Figure 4.2.: The intensity distribution of two point sources on the image plane. a) object points are clearly resolvable b) Rayleigh criterion: limit of resolution c) the object points are not resolvable and look like a single (blurred) point source.

5. Charge Coupled Device (CCD)

This chapter explains properties of CCDs in general and for the used cameras in specific.

5.1. General description of CCDs

As the camera is an important and often critical component in an imaging system, this section will deal with the properties of a Charge Coupled Device (CCD). The different camera types will be mentioned, how images are recorded will be briefly described and a description of the noise sources will be emphasized.

5.1.1. Characteristics of a detector

The largest amount of electrons a pixel can hold before the quantitative quality of the sensor diminishes is named **full well capacity**. When a pixel becomes saturated reaching its full well capacity the exceeding charge fills adjacent pixels and the camera differs from a linear response. This smearing effect is called **blooming**.

Closely connected to the full well capacity is the **dynamic range**. It describes the range between lowest light signal and highest light signals that can be detected. The dynamic range is defined as full well capacity divided by the readout noise and is often written in Decibels.

The **frame rate** is the fastest rate pictures can be recorded at in terms of full frames. The value depends on the number of pixels and the readout rate. It can be modified by implementing sub arrays or using binning. While binning (the merging of pixels into groups) is no option in our application, we use frame transfer mode[1] to shorten the time between taking two images.

The **pixel size** influences some of the detectors properties. Larger pixels degrades the spatial resolution, but has higher values concerning the full well capacity and the dynamic range.

5.1.2. Camera Types

There are several models of high-performance digital cameras on the market. The different types have different strengths and weaknesses which will be described in short. For a detailed explanation see, for example, [20] . A *CCD* (Charge Coupled Device) has only one amplifier and a serial readout device and thus shows low noise only for slow readout. CCDs are used for high sensitivity and dynamic range images. A *CMOS*

[1] For an explanation of frame transfer mode see paragraph 'Sensor Architectures' on page 24.

(Complementary Metal Oxide Semiconductor) has a parallel thus a fast readout. However, the detector needs further development because the amplifiers can vary in their properties, like in gain[2] or noise. The *EMCCD* (Electron Multiplying Charge Coupled Device) shifts the charge through a multiplication register where the charge is amplified before it is readout. This means a higher sensitivity as weak signals are separated from noise. This technique is used where high sensitivity at high speed is interesting. An *ICCD* (Image Intensified Charge Coupled Device) consists of a photo diode with a micro-channel-plate. The signal is detected by a CCD. This method is also called electron bombardment charge coupled device. Hybrid sensors combining CCD and CMOS detectors are currently in development and should be available on the market in the near future.

5.1.3. Sensor Architectures

At **full frame mode** the incoming photons shine onto the full light sensitive array and is shifted row by row to the serial output register. Then the lines are shifted horizontally and the pixels are readout one by one. This process is called 'progressive scan'. A disadvantage is the charge-smearing when light shines on the array during the readout. A shutter can help to black out the disturbing light beam, although, mechanical shutters tend to be very slow. Another possibility is to use pulsed light sources. **Frame transfer** means that the detector is separated into two areas. While one part is covered by a black out material, the other is exposed to the light. The information is transfered to the covered area where the signal is readout. This technique has a faster frame rate at the same sensitivity as the full frame type. Typically, the frame transfer is more expensive because you need twice the detector size as you like to expose. An **interline mask** is added to the photo diode (to each pixel). The mask is used for temporary storage and readout of the signal. As taking the image is a fast process here, the charge-smearing can be canceled. A shortcoming of the system is the reduced light sensitivity. Nevertheless, it is a nice method for parallel illumination (large f/# [3]).

5.1.4. Quantum Efficiency (QE)

The QE is the ratio between the photons hitting the detector and the electrons produced by them. An ideal detector would generate one electron for every incoming photon, the quantum efficiency in this case would be one. Generally, the QE depends on the construction type of the detector, the properties of the detector material (silicon), the wavelength of the incoming light and the temperature.

A front-illuminated CCD has the gate electrodes in front of the depletion region where the photons are counted. The incoming photons can be absorbed by the electrodes before entering the depletion region. The too early absorbed photons are then missing in the

[2] Gain is the amplification of the signal. Default value is 1. High gain raises noise.

[3] The f-number ($f/\#$) of a lens is the ratio of the focal length f to the aperture of the lens. The aperture is the diameter of the lens where the skew rays still may pass. Small values of the f-number mean good light-collection ability of the lens.

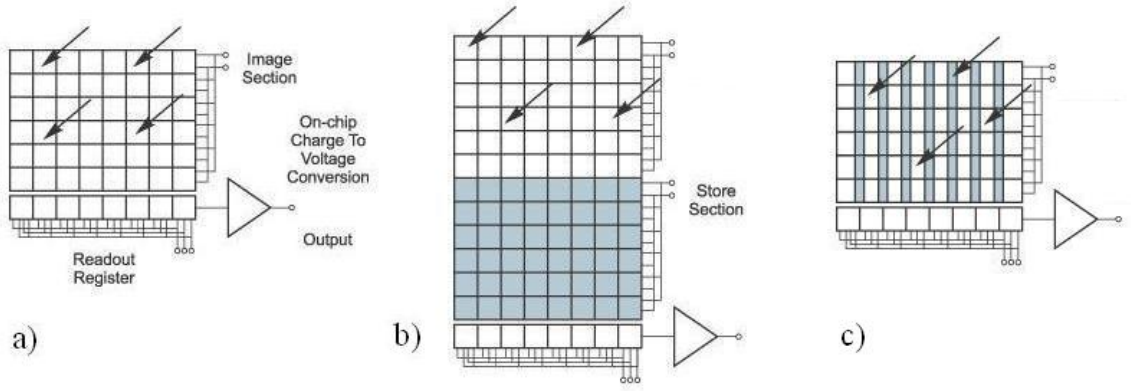

Figure 5.1.: a) Full frame transfer b) Frame transfer c) Interline mask. *Picture source: Andor [21]*

measured signal. At a back-illuminated CCD this loss is canceled because the gate electrode structure is behind the depletion region. This technology is said to minimize fringing effects. As back-illuminated cameras are expensive, efforts are made to get cheaper detectors with good QE due to transparent gate electrode materials.

5.1.5. Noise

The noise detected by a camera is the following

$$\alpha_{total} = \sqrt{\alpha_{readout}^2 + \alpha_{dark}^2 + \alpha_{signal}^2} \tag{5.1}$$

where $\alpha_{readout}$ corresponds to the sensor readout noise, α_{dark} to the thermal noise and α_{signal} to the photon noise. The **readout noise** is caused by amplifying the counted photoelectrons and converting them into a voltage. The faster the readout takes place the higher is this noise signal. Usually this noise is which limits the sensitivity of the detector. The **dark noise** originates in thermally produced electrons within the detector region. It follows the equation $\alpha_{dark} = \sqrt{N_{dark}}$, N_{dark} is the charge due to thermal effects. The higher the temperature the more dark electrons are produced. Todays CCDs produce less then 10 electrons per pixel at room temperature. Even so cooling the detector is essential for achieving good pictures. The **signal noise** is given by the nature of the light source and for a laser it follows Poisson statistics $\alpha_{signal} = \sqrt{N_{QE} \cdot P}$ where N_{QE} is the signal which is generated by N electrons in a pixel with quantum efficiency QE and P is the number of photons. This calculated noise corresponds to the average noise. As the peak values can be 5 times higher, the signal should be considerably higher than the average noise level.

5.1.6. Nyquist theorem

The theorem of Nyquist and Shannon states that a signal frequency ν can only be sampled correctly if it is equal or below one half of the sampling frequency ν_S [22, 23, 24, 25].

$$\nu \leq \frac{\nu_S}{2} \tag{5.2}$$

$$\nu_N = \frac{\nu_S}{2} \tag{5.3}$$

The Nyquist frequency ν_N is the limit frequency where a signal is still displayed accurately. In terms of imaging an object with a CCD detector it means the following. A CCD detector consists of pixels with a discrete size. The pixel spacing is given by the center-to-center distance of the pixels in image space. The sampling frequency is indirectly proportional to the pixel spacing. The pixel spacing can hence be calculated by the magnification of the system divided by the physical pixel size. Spatial frequencies greater than the half of the pixel frequency cannot be imaged any more. In terms of object space this means that two object points have to be separated a distance at least two times of the pixel size that they can be identified as two different points. Otherwise one cannot distinguish them from one object of bigger size.

In the case of the Andor camera the spatial frequency is

$$\nu_{Andor} = \frac{M}{PS} = 0.538\frac{1}{\mu m} \tag{5.4}$$

with magnification $M = 5.62$ and a pixel size $PS = 13\mu m$ and the Nyquist limit is

$$\nu_{N,Andor} = 0.269\frac{1}{\mu m} \tag{5.5}$$

.

Two terms that often come up when dealing with sampling effects are oversampling and Sub-Nyquist-sampling. Oversampling means that a sampling frequency is used which is bigger than two times the Nyquist frequency. In that case no additional information can be gained in respect to the original signal. Aliasing effects may occur so structures can be seen which are not part of the original image. In some cases (i.e. for radios) it can be useful to choose a sampling frequency which is too low and as a result intentionally lose some frequencies. This procedure is called Sub-Nyquist-sampling.

5.2. Camera Data

5.2.1. Andor iKon-M Camera

The camera we use is an iKon-M 934 BR-DD from Andor Technology[4] and for convenience will be called Andor camera from now on. It is a back-illuminated deep depletion CCD camera which is recommended for observing BECs.

[4]Further specifications can be found in [26].

Active Pixels	1024 x 1024	
Pixel Size	13 x 13	μm
Image Area	13.3 x 13.3	mm
Digitization	16	bit

Table 5.1.: Specifications Andor

Gain	A/D Rate	Counts	A/D Rate	Counts	A/D Rate	Counts
x1		583		1045		1084
x2	50 kHz	1694	1 MHz	2175	2.5 MHz	2257
x4		3811		4280		4141

Table 5.2.: Base level Andor camera. Every pixel has an offset count value. Depending on the settings the detector will display the given counts at zero exposure. This offset allows that noise fluctuations can also be accounted for if they are negative.

The camera model has a 16 bit analog-digital conversion. The typical frame rate is 2.25 frames per second for a readout rate of 2.5 MHz and 1x1 binning[5]. The produced electrons per count and the readout noise depend on the camera setting. The electrons per count ranges from 5.3 to 1.1; the readout noise from 13.7 to 2.9 electrons per pixel. Table 5.3 gives an overview over the different values and their corresponding settings. The full well capacity is 63,707 electrons corresponding to 12,020 counts for low sensitivity[6] and 57,915 counts for high sensitivity setting. Thus, the dynamic range lies between 4,650 (= 73 dB) for the lowest sensitivity and 21,968 (= 87 dB) for the highest sensitivity.

Also to be found in table 5.2 are the base levels which are fixed offset values for each pixel. The base level is important to make sure that negative noise values can also be seen.

Dark Current: The producer of our camera recommends an operating temperature of at least -65°C which can be achieved by air cooling.

The 'BR-DD' in the camera's name indicates that the model is a back-illuminated CCD with a deep depletion region. The result of this construction method is a high quantum efficiency (see figure 5.2). A measurement of the QE can be found in the passage 5.2.4.

[5]The frame rate decreases for lower readout rates and increases for higher binning.
[6]The term sensitivity alludes to the corresponding settings given in table 5.3.

A/D Rate	Gain	Sensitivity in electrons/count	Readout Noise for Single Pixel in electrons
50 kHz	x1	5.3	5.3
	x2	2.7	3.5
	x4	1.3	2.9
1 MHz	x1	4.8	13.1
	x2	2.4	8.7
	x4	1.3	6.8
2.5 MHz	x1	4.6	13.7
	x2	2.4	10.0
	x4	1.1	8.8

Table 5.3.: Sensitivity and readout noise for different Andor settings. The sensitivity shows how many electrons are produced when detecting a photon. The readout noise is a combination of CCD readout noise and A/D noise. The readout noise states the mean value of electrons which are produced without exposure to light on a single pixel. These values may differ with temperature, exposure time and when using binning options.

RT	> 1000	e^-/(pixel sec)
-60 °C	1	e^-/(pixel sec)
-80 °C	0.01	e^-/(pixel sec)
-100 °C	0.0005	e^-/(pixel sec)

Table 5.4.: Dark current Andor. The dark current strongly depends on the temperature of the detector. Cooling is urgently required and can be realized with air or water.

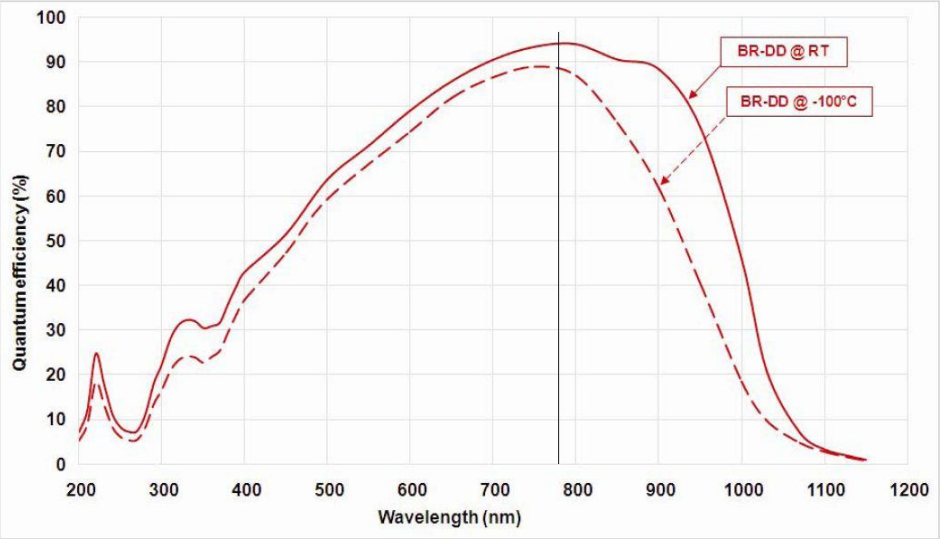

Figure 5.2.: Quantum efficiency of the iKon-M camera according to its manual, BR-DD stands for the used detector type: back-illuminated deep depletion region. The line marks the used wavelength of 780 nm. *Picture source: [26]*

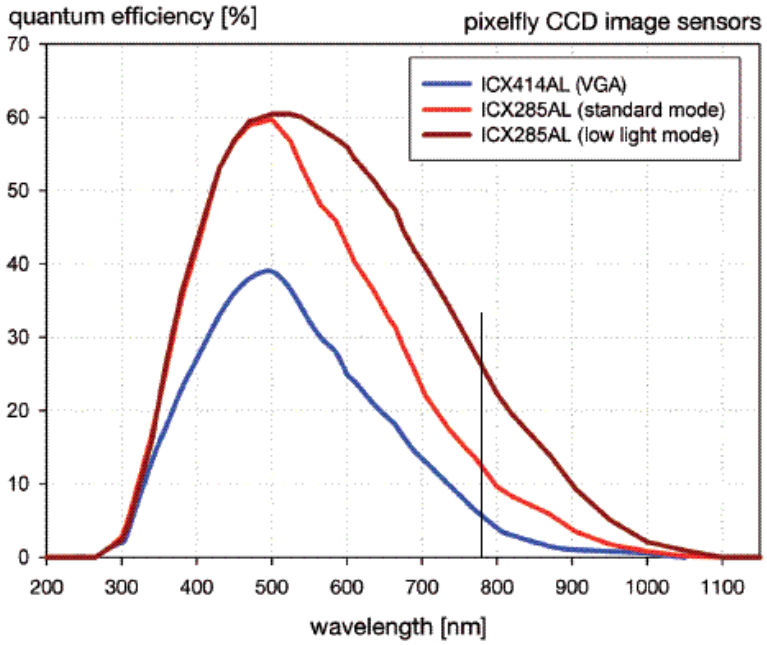

Figure 5.3.: Quantum efficiency of the Pixelfly camera according to its manual. The line marks the used wavelength of 780 nm. *Picture source: [27]*

5.2.2. Pixelfly Camera

The other camera in the setup is the Pixelfly-qe from the company PCO, which was already present in the old setup. Further on the camera will be called Pixelfly. The digitization is 12 bit, the frames per second transmitted (per chance also) 12.

The detector produces 3.8 electrons per count and has a readout noise of 9 electrons per pixel. The given full well capacity of 18,000 electrons corresponds to about 4,700 counts. The dynamic range calculated by these sizes is found to be 2,000 (= 66 dB). In figure 5.3 the theoretic at value of the quantum efficiency at a laser wavelength of 780 nm can be found to be below 30%.

The camera measures 1392 x 1024 pixels with a pixel size of 6.45 μm.

5.2.3. Differences of the cameras

The Pixelfly camera of the former imaging system is inherited for its bigger effective detector size as it implies a greater field of view (see fig. 5.4). But the quantum efficiency is very low, in fact the camera detects only every third photon. As advantage can be taken that the camera can be exposed to larger light intensities even if the full well capacity is lower than that of the Andor camera. On the other hand the Andor camera is rightly called light sensitive. With a quantum efficiency clearly above 90 % nearly every incoming photon gets detected.

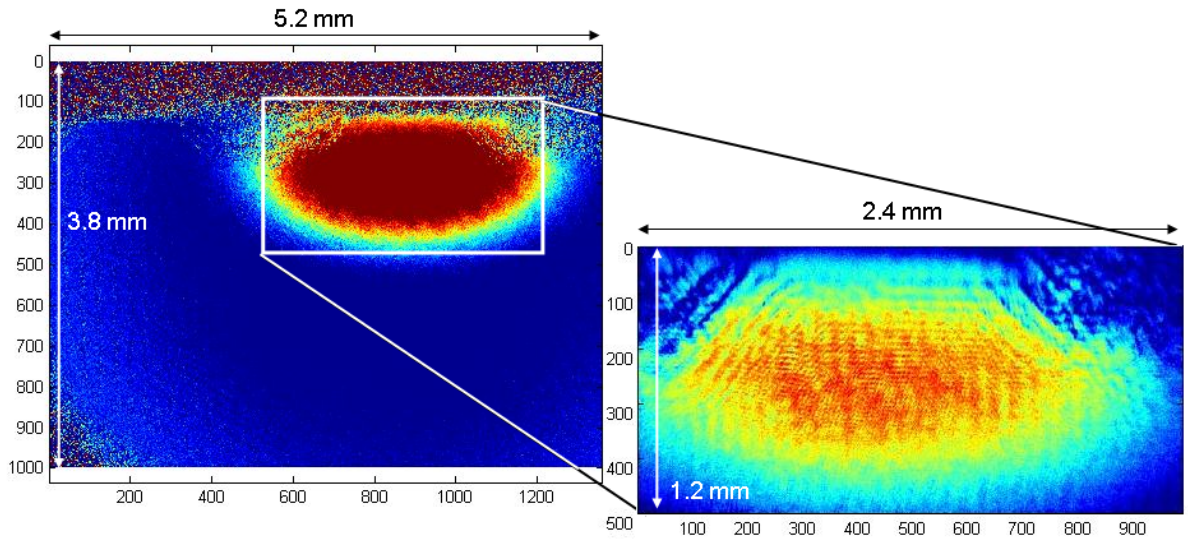

Figure 5.4.: Comparison of the imaging regions. Left: Pixelfly imaging area. Right: Andor imaging area. *Axes are pixel.*

5.2.4. Measurement of the Quantum Efficiency

To verify the specified QE value of the manual, we compared the intensity measured with a power meter to the counts produced with the camera detector. The uncertainty of the power meter given in the specification sheet is 3%.

The energy of a photon is $E_{photon} = \hbar\omega = h\nu = \frac{hc}{\lambda} = 2.5467..\cdot 10^{-19} J$ with the Planck constant $\hbar$, the velocity of the light c and the wavelength of the used laser light $\lambda =$ 780 nm. For example, a measured intensity of 1 nW equals to a number of about $4 \cdot 10^9$ photons.

The result of the comparison of power meter to CCD, however, was very unsatisfying as the QE calculated was 36 %. A discussion of the bad results lead to two difficulties in the measurement: Areas of high intensity are overexposed and hence fewer photons were counted than obtained. Areas of low intensity cannot be easily distinguished from the background signal. Taking these concerns into account an area could be found where the measured quantum efficiency yielded to 95% ± 12%. The quantum efficiency stated by the manufacturer is 92% at $780nm$, as can be found in figure 5.2.

A measurement for the Pixelfly camera yields to the actual quantum efficiency of 27% ± 2%, compared to a specified value of ≈ 27%.

5.3. Data Acquisition

The imaging cycle is embedded in the Adwin system which is the basic control program within this workgroup and widely spread in the ultra cold-atoms community. Andor provides means of control over the camera not only by user interface but also with a software development kit (Andor SDK [28]).

acquisition mode	fast kinetics
trigger	external
exposure time	3 ms
shifting speed	5.775 ms
readout rate	50 kHz
gain factor	4
imaging height	512 pixel
number of series	2

Table 5.5.: The used settings for the Andor camera.

Whether the user interface or an acquisition program is used one has to know very well which settings one like to apply. The user can choose between several acquisition modes. The most simple one is called **single acquisition** which will take only one image at a time. The **accumulate mode** takes several images at once which enhances the signal to noise ratio. The kinetics mode and fast kinetics mode seem similar to the accumulation mode at the first glance as several pictures are taken with one trigger signal. But the accumulation mode adds the individual pictures to a data set while the **kinetics mode** shows a time evolution of consecutive pictures. The system is limited to a minimum exposure time. The very smallest exposure times can be achieved with the **fast kinetics mode**. The downside of this method is that not the whole detector size can be exploited. In fast kinetics mode only a part of the detector is exposed to light and the image shifted onto the dark region of the chip[7]. So what ultimately limits the exposure time is the shifting speed of the CCD chip. The signal is readout either when the defined number of pictures is stored or the storage area is full. The user has to make sure that the CCD chip is only exposed where it is wanted. In our experiment we used this fast kinetics mode and covered the storage area of the CCD detection region with black cardboard. The necessary parameters for the different modes can be found in [29] on page 56ff.

The internal camera shutter takes a relatively long time to open and close which turned out to disturb a correct image acquisition. To solve this problem the exposure time of the camera is set higher than the laser pulse duration. The real image exposure time is then given by the acousto-optical modulator of the laser beam.

[7] See also frame transfer architecture on page 24.

6. Ray tracing

Nowadays optical design software is a mighty and commonly used tool for calculation of the desired lens setup, optimizations and performance analysis. Criteria for the performance are all types of aberrations. Important attributes are the maximum spot size on the image plane (point spread function, PSF) and the modulation transfer function (MTF).

A picture is built by the interaction of light rays. To calculate the image the ray tracing method is used. Ray tracing means that based on different object points the emitted rays are tracked through every single surface. Every ray has a determined initial direction. The calculation can be done by exact trigonometric calculation or by approximate formulas. The exact trigonometric calculation gets difficult if the system is not rotationally symmetric (e.g. aspheric lenses). Fortunately, there are plenty of ray tracing programs on the market. Ray tracing programs not only help to model a setup but also to analyze and optimize it. In the case of this diploma thesis, the ray tracing program Zemax was used for creating and testing the optical design. Zemax has the reputation to be a very user friendly program and thence was the means of choice.

There are two basic options when designing with **Zemax**. The 'sequential ray tracing' mode calculates surface after surface in the given order. It is a numerically fast calculation and is used also for design, optimization and tolerancing calculations as it is for aberration calculations. But it is not possible to attend to stray light or multiple ray paths. If you need to take several light sources into account or wish to design interferometers, for example, there is another program branch to do this. The 'non-sequential ray tracing' mode traces a ray without a pre-defined path. The ray may reflect, diffract, split into two and so on. The calculation is slower than in sequential mode. A sequential design may be converted into a non-sequential design but not the other way around.

6.1. Getting started with Zemax

A weakness of Zemax is the version management. Changes cannot automatically be undone. So you need to save the file often and keep track of its contents yourself.

The first tasks for a design project in Zemax are typing in a few factors, so Zemax is able to do the calculation. These values are found in the menus System/General, System/Fields and System/Wavelengths. Two main values at General are the entrance pupil diameter and the unit setting. At Fields you may choose where the rays originates (on-axis or off-axis), the default setting is an on-axis-source with x-field zero and y-field zero. At Wavelengths you set the wavelength of the used light. This is important for the proper calculation through the different lenses. The program provides many tools and

functions and not all of them will be explained here, although you should get familiar with them if you try to design an imaging system. Nonetheless, some features will be picked out and presented in this section.

Tools/Lens Catalogs gives you a catalog of the known lenses which can be ordered at the different manufacturers. Assure yourself that the catalogs are up to date. With Tools/Reverse Elements you are able to flip the lens. Tools/Slider is a nice method to visualize what changes of certain values do to the system.

Important for optimizing the system is the Merit Function Editor. There the parameters are set which will be optimized during an optimization cycle. It can be controlled either directly or via the Tool/Default Merit Function (within the window of the Merit Function Editor). The latter is sufficient for optimizing on a small spot radius hence a good focus. If you need to add special properties which should be taken into account, please find an explanation of the different variables of the Merit Function in the Appendix of [30]. If some distances cannot be changed (as for example the size of the vacuum chamber in our case), be sure to fasten these parameters in your Lens Data Editor so that they will not be changed by the optimization tool.

6.2. Analyzing Aberrations with Zemax

A question was ignored until now. This question is: How do we know which kind of aberration we are dealing with? Zemax offers two tools to analyze a given system for its aberrations. These tools are called ray fan plot and spot diagram. In the following paragraphs you find a description of these plots as well as the appliance on specific aberrations as well as on our system[1].

6.2.1. Ray fan plot

The first thing to explain is the ray fan. We expect to have an imaging system consisting only of a point source, a single lens which has the functionality of a pupil entrance, and the image plane. The object point is considered to be off the optical axis. The tangential plane is the plane consistent of the optical axis and the point source. Perpendicular to it you find the sagittal plane. A ray fan plot can be drawn either for tangential or sagittal rays. The distribution of rays between the lower and upper marginal rays is called the ray fan. As the lens is considered to be the pupil entrance the chief ray hits the lens at its center. Following a ray a from the object source to the image plane, it traverses through the pupil entrance before reaching the image plane. The first value to be plotted is the normalized[2] position of ray a at the lens. This value is opposed by the position[3]

[1] The paragraphs are following [30]. If you like to learn more about this topic be advised to look for it in this book.

[2] Normalized by the radius of the pupil. The limits on the x-axis of the ray fan plot are therefore $\pm$ 1.

[3] Whereupon the position is once again taken in relation to the chief ray. This means that the position of the chief ray on the image plane is the zero-point of the y-axis of the ray fan plot.

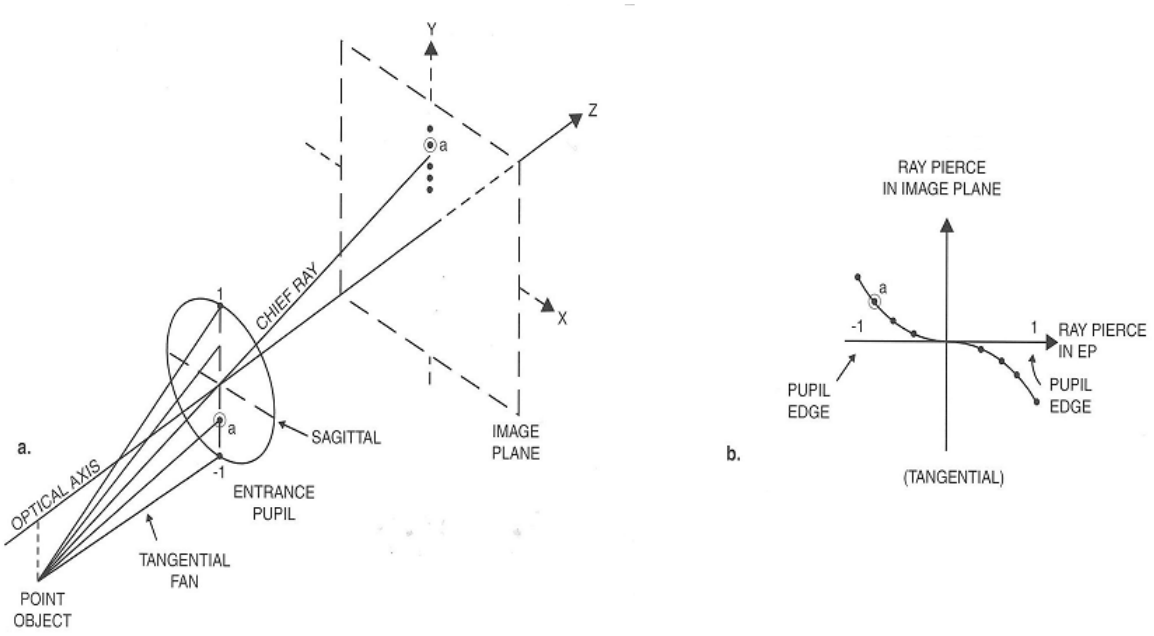

Figure 6.1.: a) The generation of the ray fan plot. b) The ray fan plot. It can be drawn in the tangential plane or perpendicular in the sagittal plane. We see here the tangential case. An off-axis object point is shone on the image plane. The different ray positions on the entrance pupil are plotted against the location on the image plane. The chief ray serves as reference point. An unaberrated system would lead to a straight line corresponding to the x-axis. *Picture Source: Introduction to Lens Design With Practical Zemax Examples* [30].

on the image plane. If the system is an ideal one without any aberrations the ray fan plot will show a straight line superposing the x-axis.

6.2.2. Spot Diagram

The spot diagram on the other hand is a plot consisting of two dimensional ray distributions. A grid is put over the entrance pupil. Rays emerging from the source hit the pupil on each grid point and is further projected onto the image plane. The arising pattern in the image plane is called spot diagram. As grid several distributions are feasible: random, square, polar, but in the most cases a uniform rectangular grid is used. The ideal spot diagram of a point source would be a single point. In the next section spot diagrams of our system can be found.

7. Design and simulation of the imaging system

While microscopes and objectives can be found on the market, the experiment nevertheless requires a custom imaging setup to meet the requirements. In figure 7.1 you find the first elements of the imaging setup. More figures including the entire setup, lens layouts and performance tests are shown later in this chapter (see table on page 39).

Mechanical constraints. For a design of an imaging system you have to take the mechanical setup and ambience requirements into account. Primary thoughts concerning the present imaging system are: How much space can be occupied at the atom chip experiment? Are there parts which should be movable? What are possible bottlenecks?

The atom cloud we wish to image is within a vacuum chamber. The vacuum chamber on the other hand is surrounded by coils which are important for the transportation of the atoms within the chamber. These coils are the reason why an imaging system cannot be arbitrarily big. The most limiting factor is the distance between two of the coils. The width of the objective there is limited to 25 mm. The finished structure has to be integrated on a 60cm x 20cm breadboard.

Further requirements. We want to use two cameras. One camera should take high resolution pictures to see fine details of the atom cloud ('Andor path'). The other camera should have a big field of view for easy navigation through the different regions of the atom chip ('Pixelfly path'). Therefore, a splitting of the beam is necessary. Even though, the cameras cannot be used simultaneously then, not a beam splitter but a flip mirror will be used for that task, as the propagation of the full light intensity is more important.

Moreover, the imaging system shall be able to image the cloud at different areas of the atom chip and it shall be able to be moved forwards and backwards in relation to the object point so it can be well adjusted to the atom cloud. On the other hand the system should be connected firmly to the surrounding parts for stability. Rather than moving the entire system, we want to move the objective only without altering the remainder of the system. To fulfill this, the objective is mounted onto a 3-D-translation-stage.

Performance requirements. What points you should consider when starting an imaging design is well explained in [31].

- *Numerical Aperture.* A crucial part of the imaging system is the numerical aperture

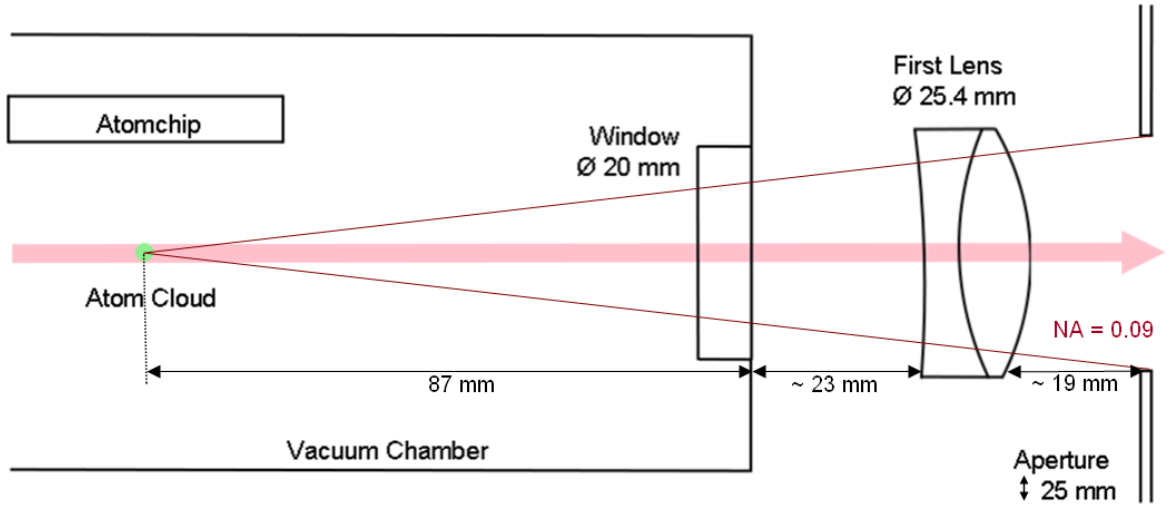

Figure 7.1.: The vacuum chamber and the first elements of the imaging system. The aperture given by two coils just outside the vacuum chamber limits the numerical aperture of the system. It is the part of the imaging system that limits the amount of light which is transfered through the system. The aperture in our case is given by two compensation coils of the atom chip setup.

NA of the system. The idea behind it is that our system should collect and propagate as much light as achievable. To increase the NA it is essential not to lose rays which managed to come out of the vacuum chamber. This means to get the first lens as near as possible to the window of the vacuum chamber.

- *Diffraction limit.* The most important property is that the system as a whole has to be diffraction limited. A diffraction limited system means that a proper reduction of aberrations is reached.

Finding a setup. The most simple setup would be a single thin lens with a given magnification and numerical aperture but for various reasons such a setup would not suffice. The cameras share the same objective but the refocusing takes place over different traces, so, a minimum of two lenses is necessary. The refocusing lens is optimized for the Andor path. That means that another lens is essential to correct the focus length onto the Pixelfly camera which is located at another distance than the Andor camera. So we now know that we need three lenses for the most simple system which still fulfills our demands. The refocusing lens shall be placed directly behind the 3-D-translation stage to improve the magnification due to gain of space (to be able to use a lens with the highest possible focal length). On the other hand, as the beam is collimated while arriving at the refocusing lens, the position of it is not sensitive to the distance to the objective and grants freedom of movement.

Zemax test runs. Keeping in mind that the window of the vacuum chamber has two coils close to it which limit the space there considerably, the first setup was sought. The first step in finding the new imaging system is to find the objective for it. The purpose of an objective is to collimate the incoming beam. It should collect as much light as possible coming from the imaged object. Concretely, the numerical aperture has to be observed while trying different concepts. Furthermore aberrations should be minimized. One of these requirements is that the objective has to has a minimum length given by the size of the vacuum chamber (see fig. 7.1). As the imaged object is within the vacuum chamber and the imaging system is on the outside, the minimum distance between atom cloud and the first lens is 87 mm[1]. Beyond that the objective should be as short as possible without losing performance quality. A useful trick is to consider the objective back to front. This means that a parallel beam is sent through the objective lenses. The distance between our last lens and the focus point has to be at least 87 mm. When an objective is found the sequence is flipped back to normal. Trying different lenses with different focal length ratios of objective and focusing lenses, it became clear that two objective lenses are necessary to circumvent the limited space due to the coils. With one objective lens every setup would lead either to bad aberration behavior or to the need to put the lens there where it is prevented by the coils. A solution was found by setting a lens between window and coils and putting a second lens behind the coils. The focal length of the objective resulted in about 17.5 cm.

Pushing the limits. Once a satisfying objective was found, the next step is refocusing the beam. Above all, this was a task to push limits and get as much space as possible for the beam propagation[2]. Several mirrors, a custom-made camera tower (see appendix E) hosting the Andor camera and a second level for the Pixelfly camera enabled the use of a lens with a focal length of 100 cm despite the breadboard length of 60 cm which already hosts the objective.

First results. The area occupied by two coils prevents putting even a small lens there. The tube holding the first lens, a one-inch lens, had to be cut. As it was not feasible to collimate the beam in the short distance between vacuum window and coils, the coils still cut off some rays and yield a numerical aperture of 0.091[3]. The expected magnification of the lens system according to equation 2.3 (with $b = 100cm$ and $a = 17.5cm$) is 5.7. The effective pixel size of the camera is the physical pixel size divided by the magnification. It will be about 2.3 μm.

[1] This is an assumption considering the lens is contiguous to the vacuum chamber window. Usually, this will not be the case as the window frame prevents an one-inch lens from coming closer than 5 mm. A one-half-inch lens could be located nearer to the window but it would also lower the numerical aperture significantly.

[2] As the ratio of the refocusing length to the objective length gives the magnification. Therefore it is convenient to have a long focal length for a large magnification, giving a detailed view of the cloud.

[3] see fig. 4.1: $NA \approx \frac{D}{2f}$.

On the next pages you find a multitude of figures. To simplify the navigation, a list of the figures is shown in the table below.

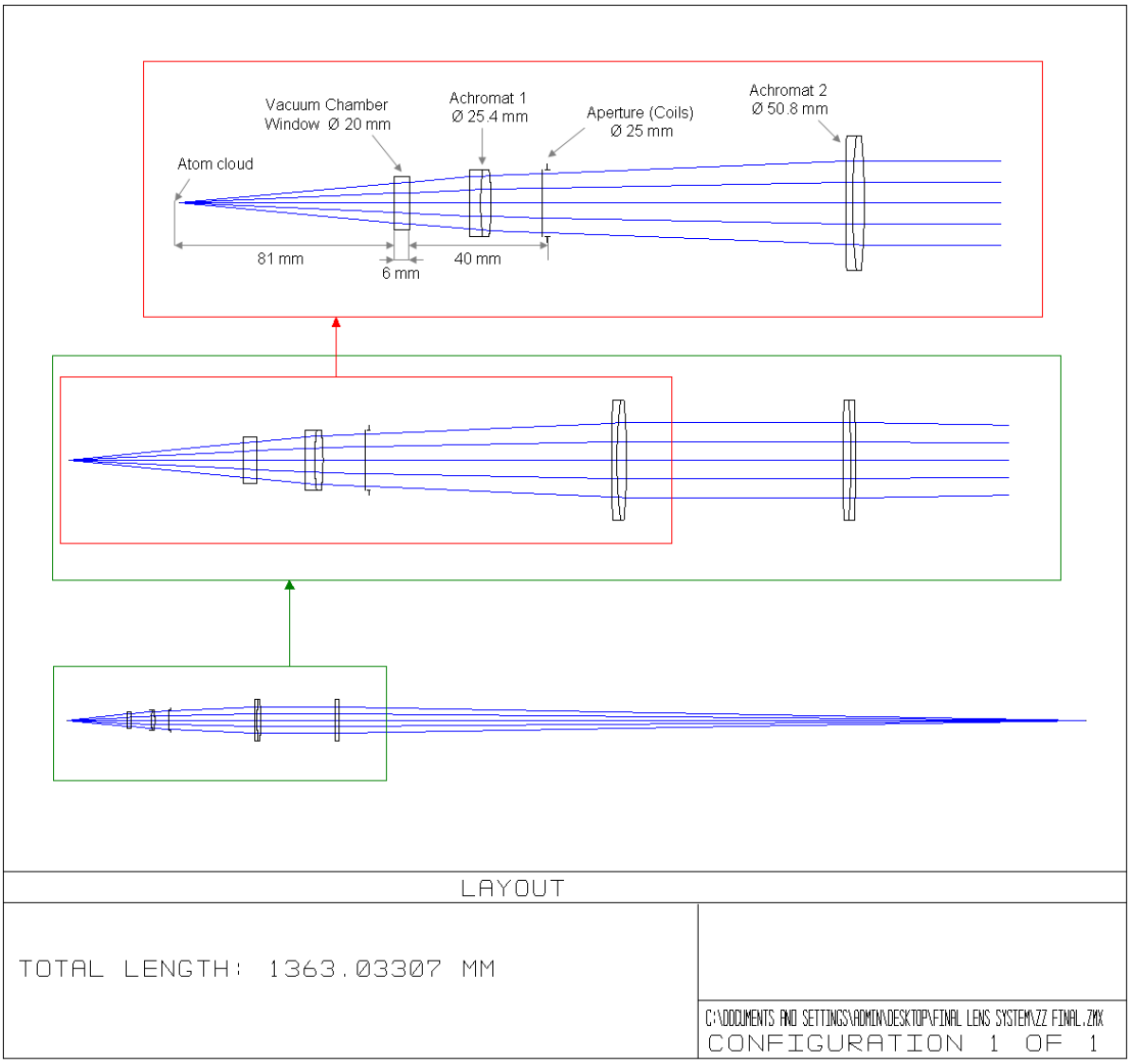

Figure 7.2.: The lens design of the imaging system at three different scales. It is 1.36 m long and consists of three achromats (see also section 2.3.3 on page 11 and table 2.1 on page 9). You find the window of the vacuum chamber at a distance of 81 mm from the cloud and the aperture of the system given by two coils at 127 mm from the atoms. Achromat 1 and achromat 2 are mounted in the same tube. As achromat 1 has a bigger diameter than the aperture, this tube had to be cut to be able to put the first lens to its proper position. The achromats of the objective (achromat 1 and achromat 2) are inserted back to front while the refocusing lens (achromat 3) is front to back because this is the setting with the best aberration correction.

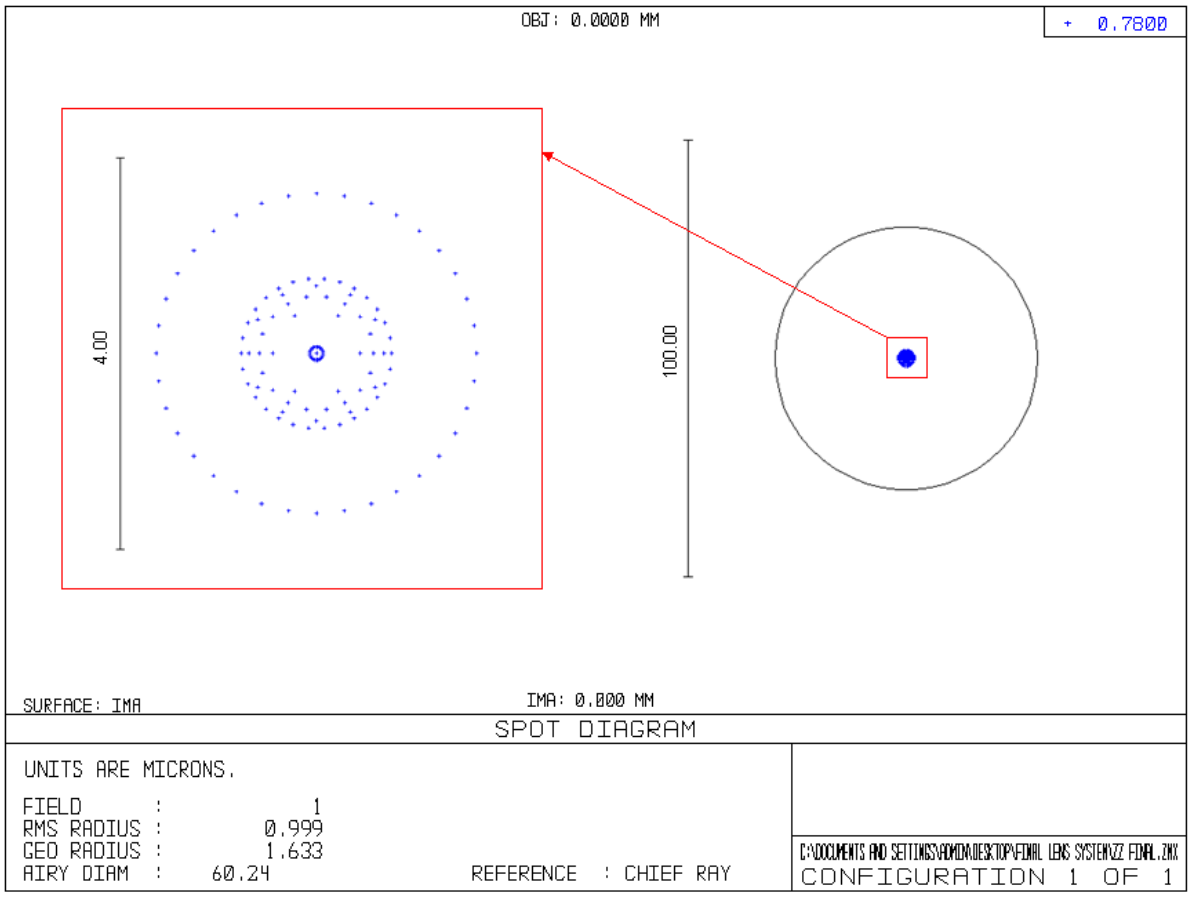

Figure 7.3.: The spot diagram of our system. Left: A close-up of the spot diagram. Right: The spot diagram (blue disk) in relation to the Airy disk (black circle).

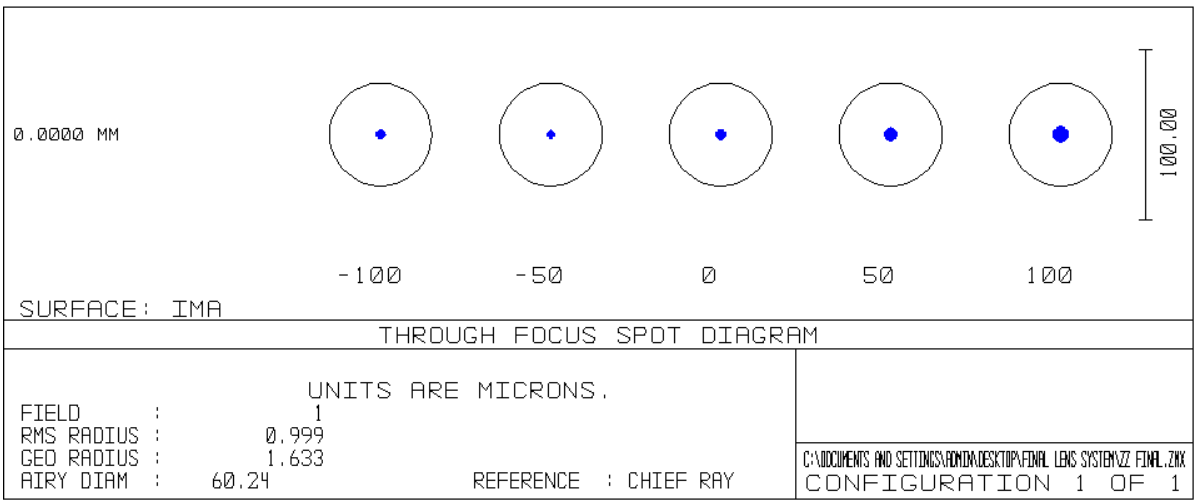

Figure 7.4.: Spot diagram and Airy disk for different image planes. The blue disk is the spot diagram of our system, the black circle the Airy disk. We see them for the focus plane (0) and different steps of defocus (-100, -50, +50, +100). All pictures are calculated for an on-axis ray (indicated by the 0 mm on the left side). The RMS radius as well as the Airy disk diameter are given for the zero defocus case. The spot of defocus -50 μm has a smaller rms radius but shows more aberrations as the focus point. *All units are μm.*

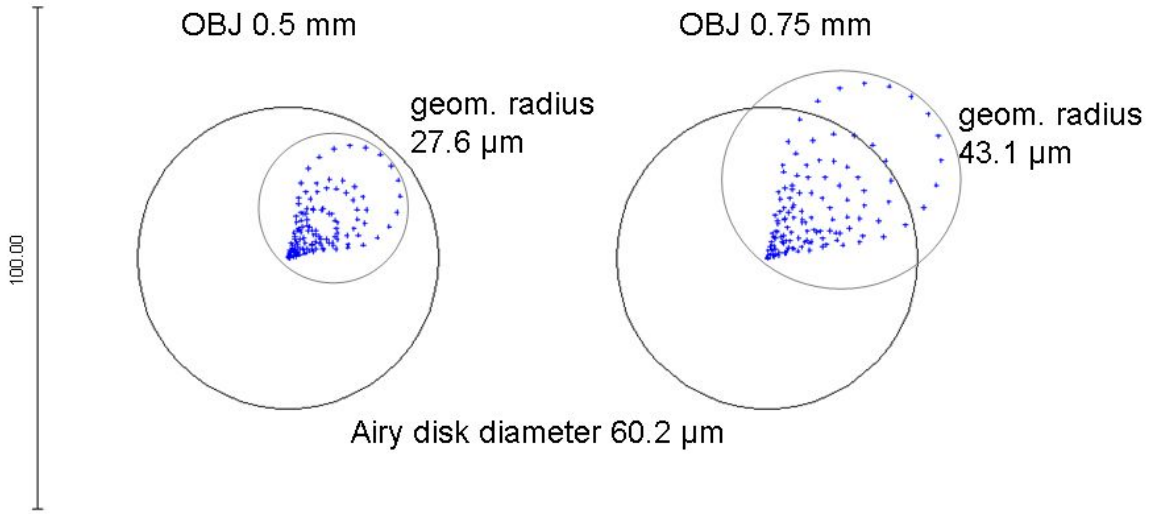

Figure 7.5.: The spot diagram of our system for off-axis rays. Left: For a ray that originates in the object space 0.5 mm off the optical axis. Right: For a ray that originates 0.75 mm off the axis. Both cases leads to coma. The left picture is still diffraction limited.

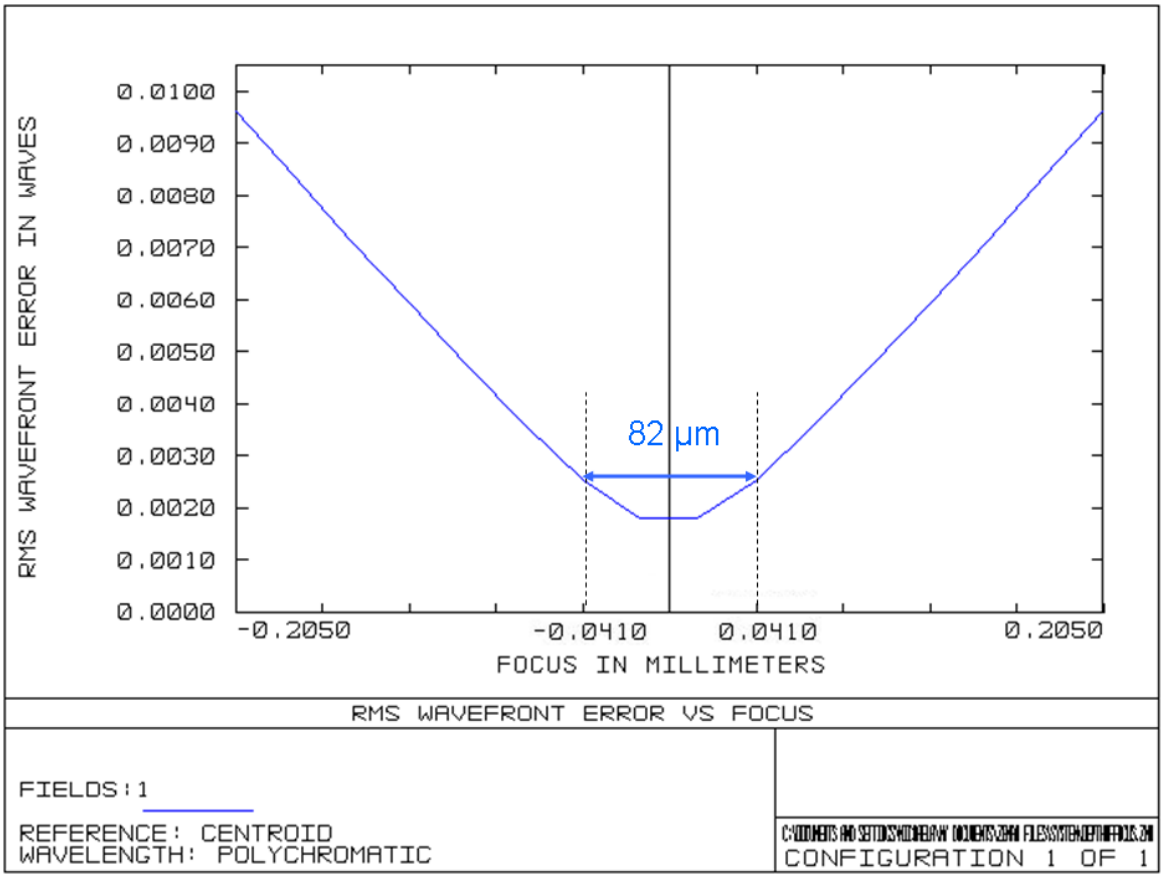

Figure 7.6.: The depth of focus is $\sqrt{2}$ times the root mean square (RMS) value of the focus point and results in 82 μm.

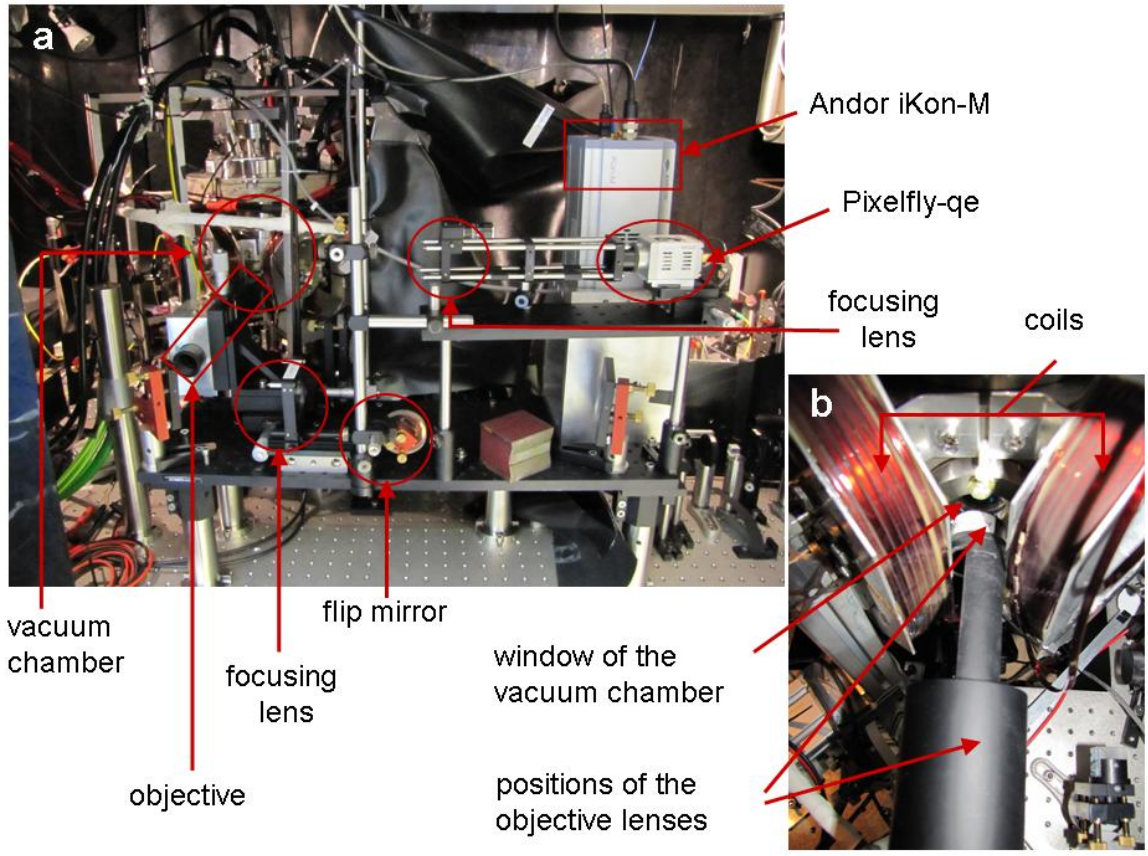

Figure 7.7.: a) Photograph of the setup. The imaging beam travels from the vacuum chamber through the objective, then hits the first mirror before reaching the focusing lens. The flip mirror in the picture is alongside the beam and allows propagation to three more mirrors (only one can be seen) and finally onto the Andor's CCD. The flip mirror need to be mechanically switched to take images with the Pixelfly camera. b) Close up picture of the objective. The black tube holds the objective lenses (one in front of the coils, the other behind the coils). The window of the vacuum chamber has a diameter of 20 mm. The front part of the lens tube has a diameter of 30 mm and has to be cut to fit in between the coils.

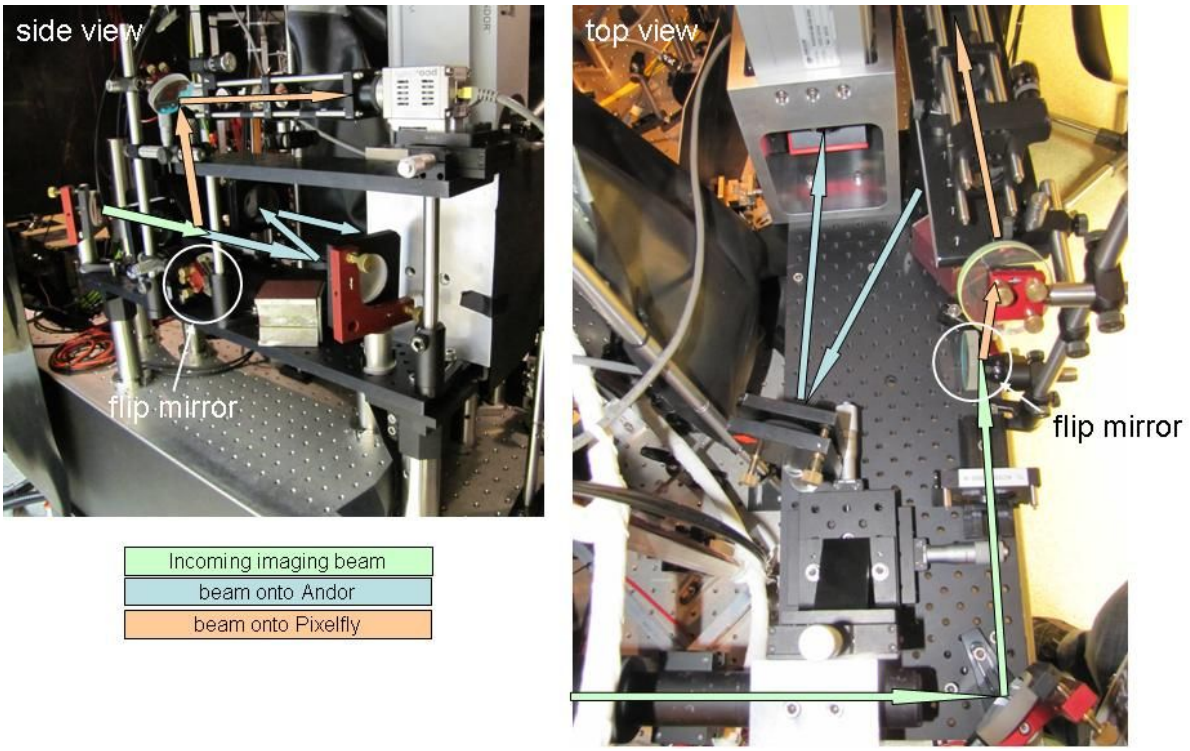

Figure 7.8.: The imaging beam propagates as indicated by the arrows. The green arrow is the course of the beam for both paths. After the flip mirror two cases are possible. Either the mirror is alongside the beam path (which is the case in this photograph) passing the beam onto the Andor camera (blue arrows), or the mirror redirects the beam onto the Pixelfly (orange arrows).

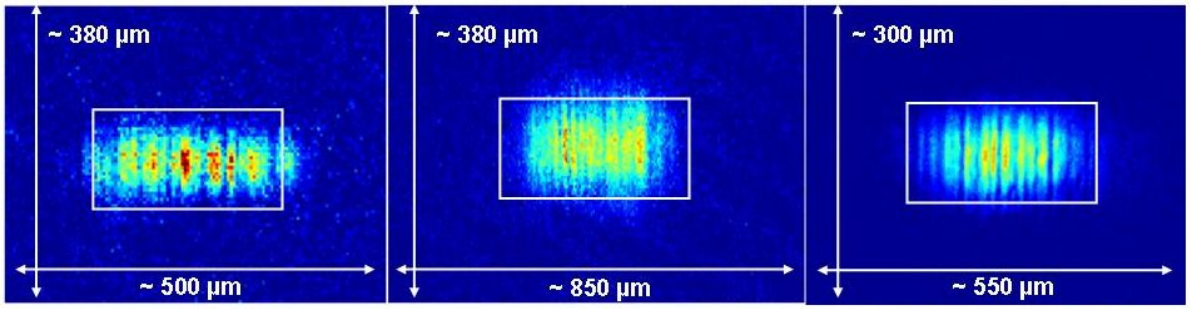

Figure 7.9.: Evolution of the imaging system. Left: BEC imaged by the old imaging setup. Middle: BEC imaged by the new setup with the Pixelfly. Right: BEC imaged by the new setup with the Andor camera. The white boxes are of the same size (100 μm x 250 μm).

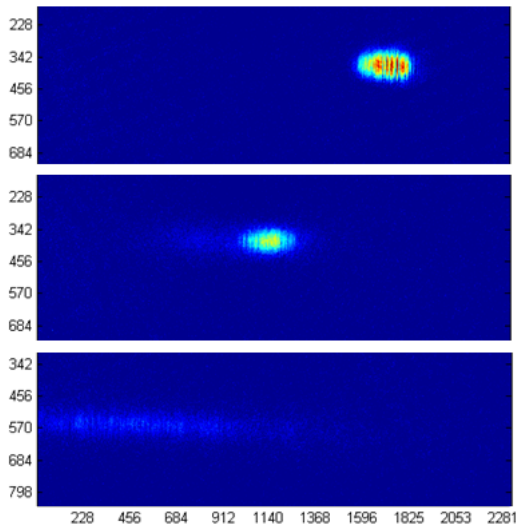

Figure 7.10.: Transport of the atom cloud. Pictures taken by Andor camera. *Axes are μm.*

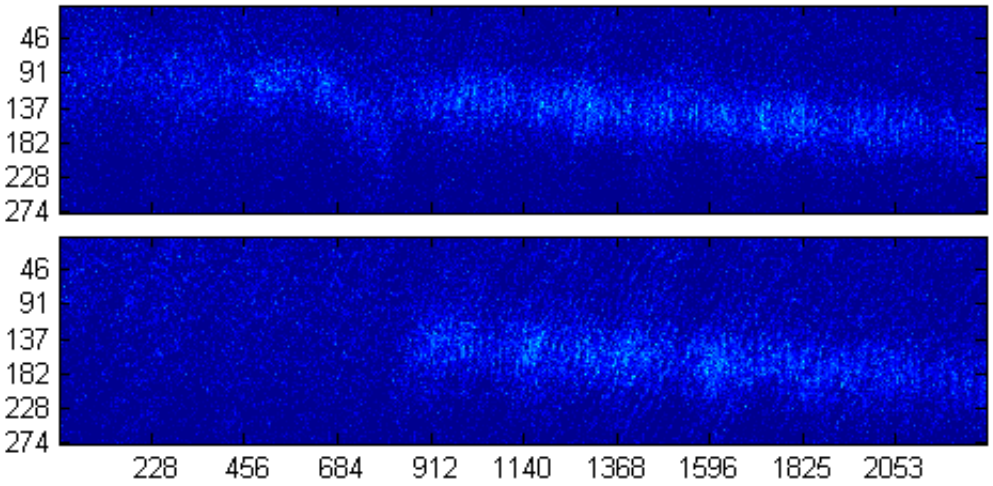

Figure 7.11.: Pictures of atoms at the fiber detector taken by the Andor camera. Upper image: detector is off. Lower image: detector is on. The atoms are heated out of the trap by the detector beam. The peak line density of the could is about 6 atoms per micrometer. The associated peak column density is 0.33 atoms per micrometer squared, which corresponds to 1.6 atoms per pixel. The atoms at this region could not be seen with the previous imaging setup. *Axes are μm.*

8. Characterization of the imaging system

8.1. Focusing

We used different methods for focusing the system and every method has its unique application area. The first alignments were carried out with a two-dimensional target (see appendix B). It was used to control the setting of the lenses relative to one another before the imaging system was built into the atom chip experiment. When the distances of the lenses were proper and fixed the imaging setup was built into the experiment and should be focused onto the atom cloud. The chosen focusing method was found in the thesis of Andreas Marte [12] and will be discussed in part 8.1.1. While this effects can be well used for in situ clouds, focusing time of flight BECs is achieved by using the effect of density ripples 8.1.2. Density ripples arise in 1-D quasicondensates as there are several phase coherent domains, but no phase coherence over the entire condensate. When the condensate is released from the trap the domains interfere with one another. A regular interference pattern means a regular length of the different domains.

8.1.1. Lensing effect

The focus has to be well aligned as the optical resolution is sensitive to it. The outcome of ill focused thermal clouds or condensates are distortions in the image. Good focus can be achieved by taking advantage of dispersive effects of the atoms. As the light absorption of the atoms depends on the wavelength of the laser beam different intensity profiles can be found for different detunings [12]. If the light is blue detuned the refractive index of the cloud is smaller than 1. Additionally, there are different beam profiles for focusing in front of the cloud and in the rear of the cloud. The negative intensities are explained with virtual negative optical densities which are caused by refraction effects. The red detuned case is complementary to the blue detuned. Intensity profiles that are found in front of the cloud (focus point too far away) for blue detuning are found in the rear of the cloud (focus point too close) for red detuning and vice versa. For large detunings the signal to noise ratio gets small and thus the effect is no longer to be seen.

8.1.2. Density ripples and focus

Insitu pictures of the cloud are taken with the magnetic fields on. The fields have a strength of 3.3 G which corresponds to a transition variation of 4.62 MHz. The found

focus point consequently is not the same focus point as for a cloud in free fall. The focus is well enough aligned all the same because the cloud has a finite size which is bigger than the shift of focus introduced by the magnetic fields. If it is necessary to adjust the focus for a time of flight measurement a possibility is the measurement of the density ripples of elongated BECs. The density ripples change with different defoci and can be interpreted with the help of their Fourier transform [32, 33, 34].

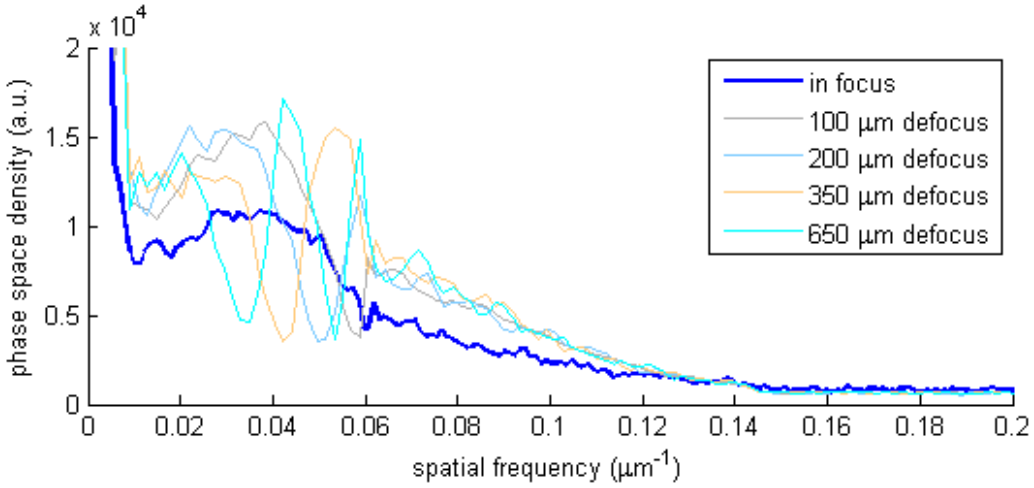

Figure 8.1.: Fourier transform of density ripples: Mean values over 50 pictures for each defocus for 12 ms TOF. The more focused the system gets, the smoother the Fourier transform becomes.

The density ripples in the atom cloud furthermore allows us to determine the resolution of the imaging system by measuring the modulation transfer function (see sec. 4.2.2). This measurement is described below in section 8.3.

8.2. Magnification

Knowing the magnification of the imaging system is central to many calculations and measurements concerning the atom experiment. The effective pixel size P_{eff} is calculated

$$P_{eff} = \frac{P}{M} \tag{8.1}$$

with the physical pixel size P and magnification M. The effective pixel size is important to nearly all measurements such as the positions of the atoms in SI units.

Zemax provides a theoretical value of the magnification but the real magnification may deviate from this value due to slight misalignments. In any case the real magnification should be determined by measurement.

To measure the magnification of the finished imaging setup the following approach was used. The trapped atom cloud is released and falls down due to gravity. The position of the center of the cloud can be determined in terms of pixels. The change of position

is plotted against the time of flight of the cloud. The trajectory can be compared to the formula of free fall. The according accelerations compared to each other gives the magnification.

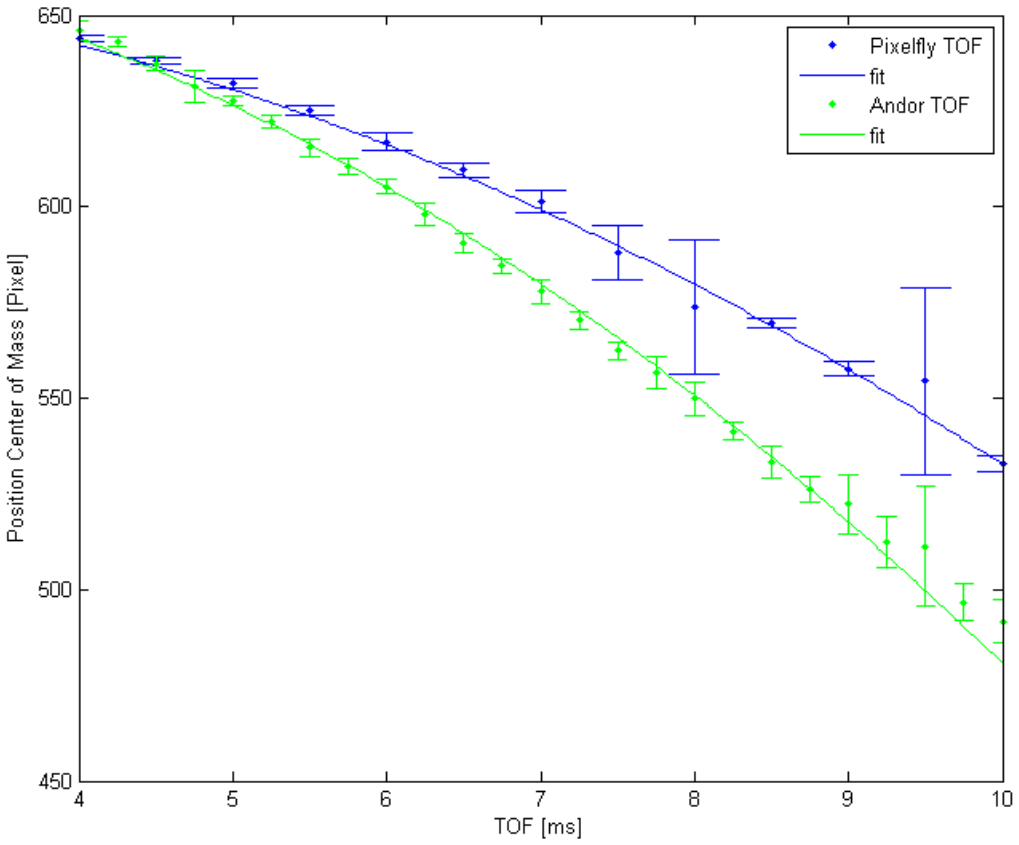

Figure 8.2.: Magnification measurement. An atom cloud is released from the trap and its fall compared to free fall. The dots are the measured positions of the cloud. The line is a simulation of free fall. You see a comparison of the free fall of the atom cloud detected with the Pixelfly camera (blue) and with the Andor camera (green). The effective pixel size of the Andor camera is smaller than the effective pixel size of the Pixelfly. (The large error bars are due to imaging interruptions.)

The measured magnification for the Andor camera is 5.62 $\pm$ 0.13 and results in an effective pixel size of 2.32 μm. The detector consists of 1024 x 1024 pixels. Consequently, the field of view is 2.37 mm^2.

With a measured magnification of 1.72 $\pm$ 0.02, the Pixelfly camera has a 5.23mm x 3.85mm effective detector size and 3.76 μm effective pixel size.

8.3. Measuring the MTF

The contrast or modulation of the system can be calculated via the measured intensities when imaging the resolution target with different grating sizes. When I_{max} is the intensity of a bright line and I_{min} is the intensity of a dark line, the contrast corresponding to the given spatial frequency k is

$$MTF(k) = \frac{I_{max}(k) - I_{min}(k)}{I_{max}(k) + I_{min}(k)}. \tag{8.2}$$

Zemax offers a calculation of the modulation transfer function. The MTF given by Zemax does not take the magnification into account. MTFs considering the magnification can be seen in figure 8.3.

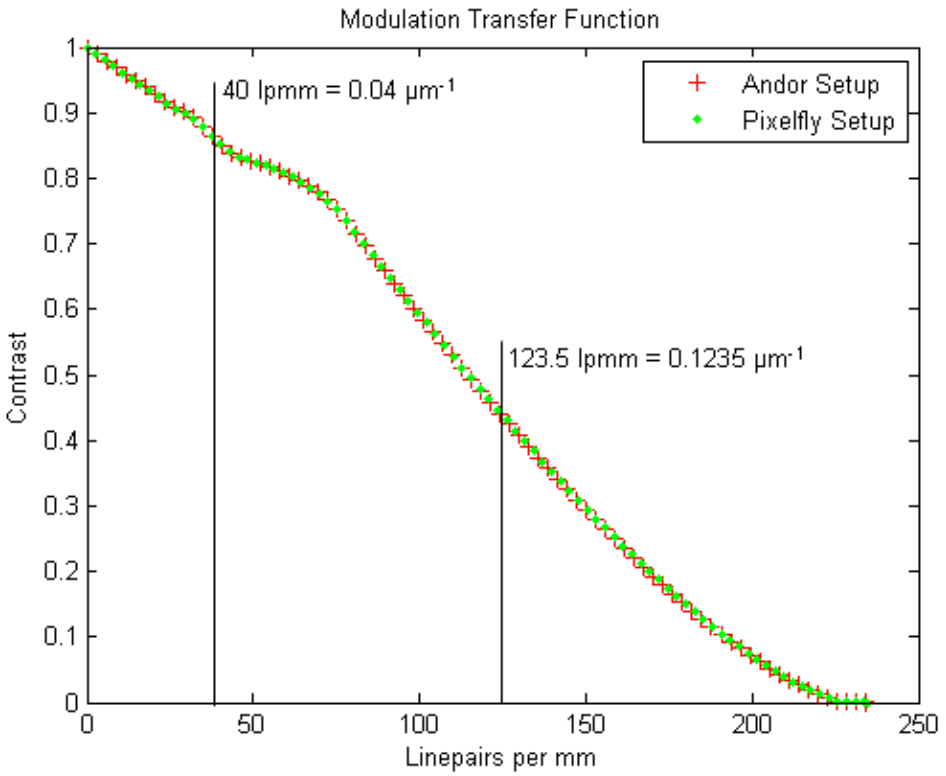

Figure 8.3.: The corrected modulation transfer function of our system. The magnification used for the correction is the theoretical value given by Zemax and may vary from the measured value (see Section Magnification). 40 and 123.5 lpmm are marked for comparison with figure 8.4.

8.3.1. Density ripples in context of MTF

The density ripples gained by a time of flight expansion of Bose Einstein condensates can be used for an analysis of the modulation transfer function. The Fourier transform of the ripples shows a cutoff frequency which is equivalent to the spatial resolution limit.

The effective modulation transfer function depends on the size of the cloud with the radius R_z in the direction of the imaging beam. A derivation of the effective MTF can be found in the appendix of [34] and consists of three terms.

$$M(\nu) = \Theta(N/\lambda - \nu)\cos(\pi\lambda\Delta\nu^2)e^{-(\pi^2/2)\lambda^2 R_z^2 \nu^4} \tag{8.3}$$

where N is the numerical aperture and $\nu = \sqrt{\nu_x^2 + \nu_y^2}$ the transversal spatial frequency. The Heaviside step function represents the diffraction limit, the second term is in account of defocus effects due to detuning and the last term describes the dependence of the resolution on the cloud thickness. The resolution becomes reduced when the cloud size exceeds the depth of focus and thence this term is important for expanding clouds. For a cloud with $R_z^{max} \sim \lambda/\pi N^2$ the system's resolution depends on depth effects and not on the diffraction limit. In figure 8.4 you find a fit corresponding to the exponential term of eq.(8.3) with $R_z = 37.8\mu m$[1]. For this case $\nu_{max} = \left(\frac{\sqrt{2}}{\pi\lambda R}\right)^{1/2} = 0.1235\mu m^{-1}$ and diffraction limited radius $R_{diff} = \frac{1.22}{2\nu_{max}} = 4.94\mu m$ which results in a measured numerical aperture (according to the Heaviside step function) of $N = \nu_{max}\lambda = 0.0963$.

[1] R_z is achieved of a Gaussian fit $e^{-z^2/(2R_z^2)}$ of the atom cloud with zero defocus and detuning. $R_z^{max} \approx 29\mu m$

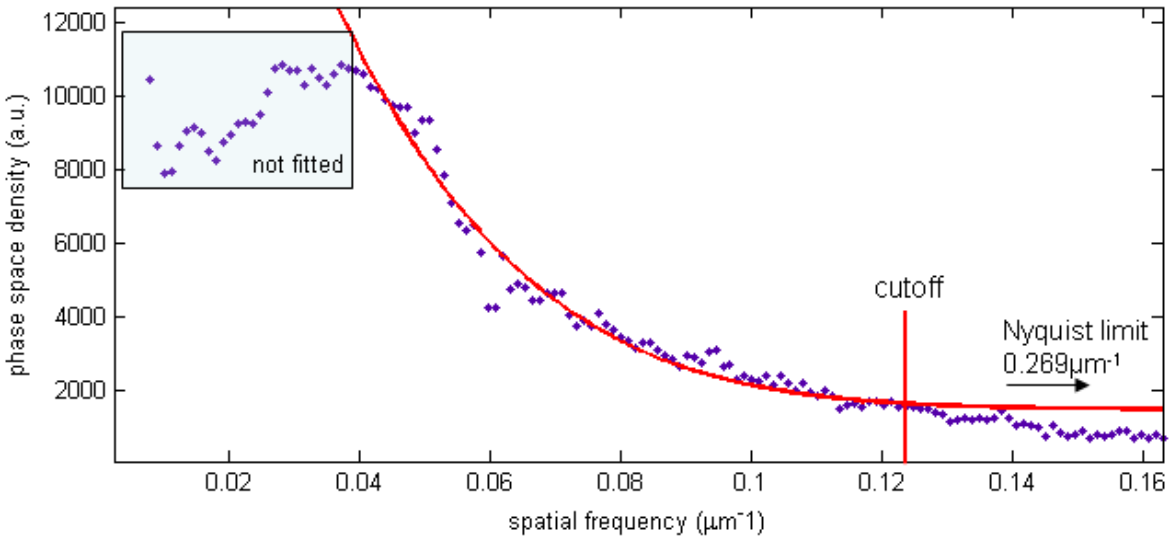

Figure 8.4.: MTF of the density ripples (dots). The resolution of the imaging system depends among others on the size of the cloud. As the cloud in TOF gets bigger, there is a chance that the size exceeds the depth of focus. The red line corresponds to the exponential term of eq.(8.3). The cutoff frequency ν_{max} is also given in the text below. The fit doesn't regard points below a spatial frequency of 0.04 μm^{-1} as this is an equivalent of structures of 25 μm or 1/10 of the atom cloud size. This means that these structures are bigger than the region of interest. (A simulation shows that the not fitted region at low frequencies is dominated by an Ornstein-Uhlenbeck distribution and consequently is not dominated by the modulation transfer function [35].).

9. Results and Conclusion

9.1. Summary of the results

In table 9.1 you find a summary of the results. The magnification was found with a time of flight measurement as described in section 8.2. The effective pixel size and the field of view are results of the magnification and the physical pixel size (page 26). The resolution limit is the Airy disk radius given by Zemax divided by the magnification. The calculated diffraction limit is gained by considerations made on page 20, the measured diffraction limit is according to page 51. The calculated numerical aperture is discussed on page 36, the measured numerical aperture on page 51. The Nyquist limit is explained on page 26.

	Andor	Pixelfly
magnification	5.62 ± 0.13	1.72 ± 0.02
effective pixel size	2.32 μm	3.76 μm
field of view	2.37mm x 2.37mm	5.23mm x 3.85mm
resolution limit	5.34 μm	unknown
diffraction limit calc.	5.22 μm	
diffraction limit meas.	4.94 μm	
numerical aperture calc.	0.091	
numerical aperture meas.	0.096	
Nyquist limit	0.269 μm^{-1}	0.133 μm^{-1}

Table 9.1.: Summary of the results

9.2. Conclusion

In this work we described the construction of a transversal absorption imaging system for a Bose-Einstein condensate for an atom chip experiment. Commercial lenses were used to build a diffraction limited imaging system. The used camera is a back illuminated deep-depletion CCD camera with high quantum efficiency and fast readout rate. Half of the detector size was blacked out to be able to acquire two images within a millisecond timescale. The characterization was carried out not only with a ray tracing program but also insitu. Different methods for focusing are presented suiting different demands (as insitu cloud, time of flight BEC). The new imaging system provides a higher sensitivity and more detailed pictures. For example, the atom cloud at the fiber detector region

of the atom chip can now be imaged. This allows a characterization of the cloud there, which was out of reach before the new imaging setup. As the results show in sec. 9.1 the system offers great prerequisites for further experiments.

Bibliography

[1] Steven Chu. The manipulation of neutral particles, Nobel Lecture 1997.

[2] Claude N. Cohen-Tannoudji. Manipulating atoms with photons, Nobel Lecture 1997.

[3] William D. Phillips. Laser cooling and trapping of neutral atoms, Nobel Lecture 1997.

[4] Albert Einstein. handwritten manuscript on bose-einstein condensates, online at www.lorentz.leidenuniv.nl, 1925.

[5] Wolfgang Ketterle. When atoms behave as waves: Bose-einstein condensation and the atom laser, Nobel Lecture 2001.

[6] Carl E. Wieman Eric A. Cornell. Bose-einstein condensation in a dilute gas; the first 70 years and some recent experiments, Nobel Lecture 2001.

[7] W.Ketterle, D.S.Durfee, and D.M. Stamper-Kurn. Making, probing and understanding bose-einstein condensates. arXiv, cond-mat:9904034v2, 1999.

[8] Dennis Heine. Single Atom Detection and Non-Classical Photon Correlations. PhD thesis, Ruperto-Carola University of Heidelberg, 2008.

[9] Marco Wilzbach. Single atom detection on an atom chip with integrated optics. PhD thesis, Ruperto-Carola University of Heidelberg, 2007.

[10] Daniel A. Steck. Rubidium 87 d line data, September 2001. Los Alamos National Laboratory.

[11] Jacob Lyman Roberts. Bose-Einstein Condensates with Tunable Atom-atom Interactions. PhD thesis, University of Colorado, 2001.

[12] Andreas Marte. Feshbach-Resonanzen bei Stößen ultrakalter Rubidiumatome. PhD thesis, Technische Universitaet Muenchen, 2003.

[13] J.C. Wyant and K. Creath. Applied Optics and Optical Engineering Basic Wavefront Aberration Theory for Optical Metrology, volume XI. Academic Press, 1992.

[14] Eugene Hecht. Optics. Addison Wesley, 4 edition, 2002.

[15] Wolfgang Demtroeder. Experimentalphysik 2. Springer, 2006.

[16] L.D. Turner, K.F.E.M. Domen, and R.E. Scholten. Diffraction-contrast imaging of cold atoms. Physical Review A, 72:031403–1 – 031403–4, 2005.

[17] Lincoln D. Turner, Karl P. Weber, David Paganin, and Robert E. Scholten. Off-resonant defocus-contrast imaging of cold atoms. Optics Letters, 29:232–234, 2004.

[18] Ramesh Neelamani, Hyeokho Choi, and Richard Baraniuk. Forward: Fourier-wavelet regularized deconvolution for ill-conditioned systems. IEEE Trans. on Signal Processing, 52:418–433, 2002.

[19] Min Gu. Advanced Optical Imaging Theory. Springer, 2000.

[20] Chin. Digital camera fundamentals. Andor Technology.

[21] AndorTechnology. www.andor.com/learning.

[22] Robert Bücker. Fluorescence imaging of ultracold atoms. Master's thesis, University of Heidelberg, 2007.

[23] Barabara Stix. A new imaging system for dual-species atomchip experiments. Master's thesis, Vienna University of Technology, 2008.

[24] H. Nyquist. Certain topics in telegraph transmission theory. Transactions of the AIEE, 47:617–644, 1928.

[25] Claude E. Shannon. Communication in the presence of noise. Proceedings of the IEEE, 72:1192, 1984.

[26] AndorTechnology. iKon-M 934 BR-DD. Andor Technology.

[27] PCO. Datasheet pixelfly qe.

[28] AndorTechnology. Users Guide to Andor SDK.

[29] AndorTechnology. Users Guide Andor iKon-M. Andor Technology, Aug 2008.

[30] Joseph M. Geary. Introduction to Lens Design With Practical Zemax Examples. Willmann-Bell, Inc., 2002.

[31] Gerd Litfin. Technische Optik in der Praxis. Springer, 2005.

[32] A. Imambekow, I. E. Mazets, D. S. Petrov, V. Gritsev, S. Manz, S. Hofferberth, T. Schumm, E. Demler, and J. Schmiedmayer. Density ripples in expanding low-dimensional gases as a probe of correlations. arXiv, cond-mat.quant-gas, 2009.

[33] S. Manz, R. Bücker, T. Betz, Ch. Koller, S. Hofferberth, I. E. Mazets, A. Imambekov, E. Demler, A. Perrin, J. Schmiedmayer, and T. Schumm. Two-point density correlations of quasicondensates in free expansion. arXiv, cond-mat.quant-gas, 2010.

[34] R. Bücker, A. Perrin, S. Manz, T. Betz, Ch. Koller, T. Plisson, J. Rottmann, T. Schumm, and J. Schmiedmayer. Single-particle-sensitive imaging of freely propagating ultracold atoms. New Journal of Physics, 11 103039, 2009.

[35] Stephanie Manz. Density correlations of expanding one-dimensional Bose gases. PhD thesis, Technische Universität Wien, 2010.

List of Figures

List of Tables

Appendix

A. Aberrations

A.1. Spherical Aberration

Spherical aberration means that rays are focused at different points along the optical axis, depending on the distance between the incoming ray and the optical axis. For a converging lens, rays hitting the lens further of the axis are focused nearer at the lens as the paraxial focal point. The spherical aberration (SA) is positive. For a diverging lens, rays hitting the lens further of the axis are focused further away as the paraxial focal point. The SA is negative. One can distinguish transversal and longitudinal SA. At the point of the paraxial focus the transversal SA is the distance to the furthest ray. The longitudinal SA is the distance between the focal point of the marginal rays and the paraxial focal point. The best image can be found at the height of minimum blur, also called circle of least confusion [14].

If strong spherical aberration is present, it can be reduced by limiting the ray with an aperture. When the aperture decreases, the circle of least confusion will move nearer to the paraxial focus. That means that you have to refocus the system when changing the aperture.

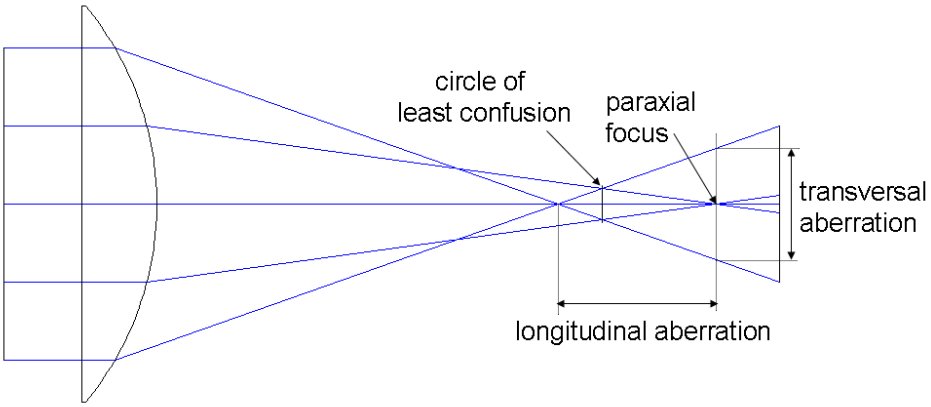

Figure A.1.: Spherical aberration. The best image is obtained at the position of the circle of least confusion.

A.2. Coma

Beam wavefronts can only be treated as planes at paraxial regions, elsewhere they are curved surfaces. For rays traveling through a lens at off-axis areas the effective focal length and the magnification deviates from the on-axis rays. If the image point is on the optical axis, coma is out of the question. But if the ray bundle is inclined and the image point off-axis coma will be present. *Negative coma:* The marginal rays hit the image plane closer to the axis than paraxial rays. The marginal rays form the smallest image (least magnification). *Positive coma:* The marginal rays focus farther away from the axis than the paraxial rays do. The image is considered to be a circular blur (Gaussian shape) for an ideal image. In case of coma there is a coma flare observed. Coma changes with the shape of a lens, with the distance to the object and can be decreased with an aperture at a proper location [14].

A.3. Astigmatism

When the object points do not lie on the optical axis the ray bundle hits the lens asymmetrically. This leads to the effect called astigmatism[1]. Distinguishing the meridional (tangential) and the sagittal plane, rays propagating in one of the planes will be focused on an other point than rays traveling in the other plane. The meridional plane contains the chief ray and the optical axis. The sagittal plane also contains the chief ray but is perpendicular to the meridional plane. Sagittal rays are skew rays that lie in the sagittal plane. For an axial object point there is no distinction between meridional and sagittal plane rays. For oblique rays the focal lengths in the meridional and the sagittal plane are different. The distance between the different positions of foci is called the focal length difference or astigmatic difference. The astigmatic difference depends on the power of the lens and the angle at which the rays are inclined (increasing for larger angles). The cross section of the beam which initially is circular will become elliptical until it degenerates into a line at the focus. One can distinguish the primary or secondary image at the tangential or sagittal focus. Between these two foci there is a location where the image blur is circular. This is the position of the circle of least confusion. The diameter of the circle increases when the focal length difference increases [14].

A.4. Field of Curvature

An image is formed on a curved surface and not on a plane one. As a CCD offers a plane detector the image will not be well focused over the whole field of view. If the system is focused on the center of the picture the outer regions will be blurred and vice versa.

[1] A very nice graphic showing astigmatism can be found in [23].

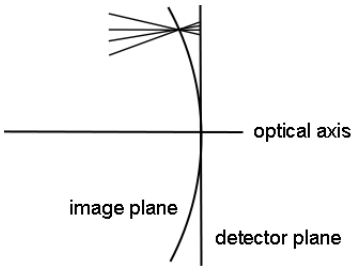

A.5. Distortion

Usually, the magnification of a system varies with the distance from the optical axis. This inherent imaging error can be shown by imaging a square. One can distinguish pincushion and barrel distortion. In the case of pincushion distortion the magnification increases with the distance, at barrel distortion the magnification decreases with the distance from the optical axis. Combinations of both distortions are referred to as mustache distortion.

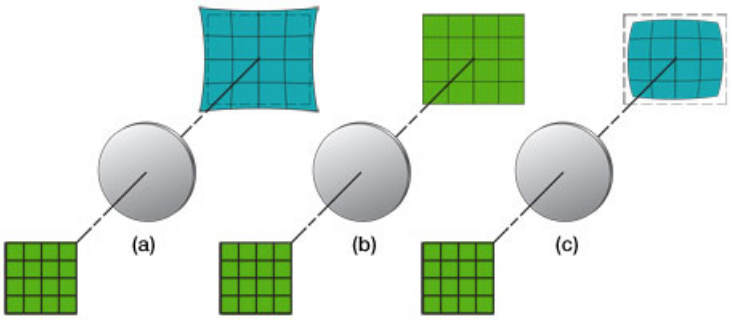

Figure A.2.: a) pincushion distortion b) undistorted object c) barrel distortion *Picture source: www.thorlabs.com*

B. Metro Chip - Microscope Calibration Target, MetroBoost

The Metro Chip allows calibration of the length scale ranging from several millimeters to submicrons. In difference to the resolution target used for first focusing exercises and measurements of the modulation transfer function, the metro chip has two dimensional structures. The structures are labeled by their pitch value. It should be noted that the periodicity, given by the pitch factor, is an accurate value, while declared width factors may deviate by up to 20 % from the real values.

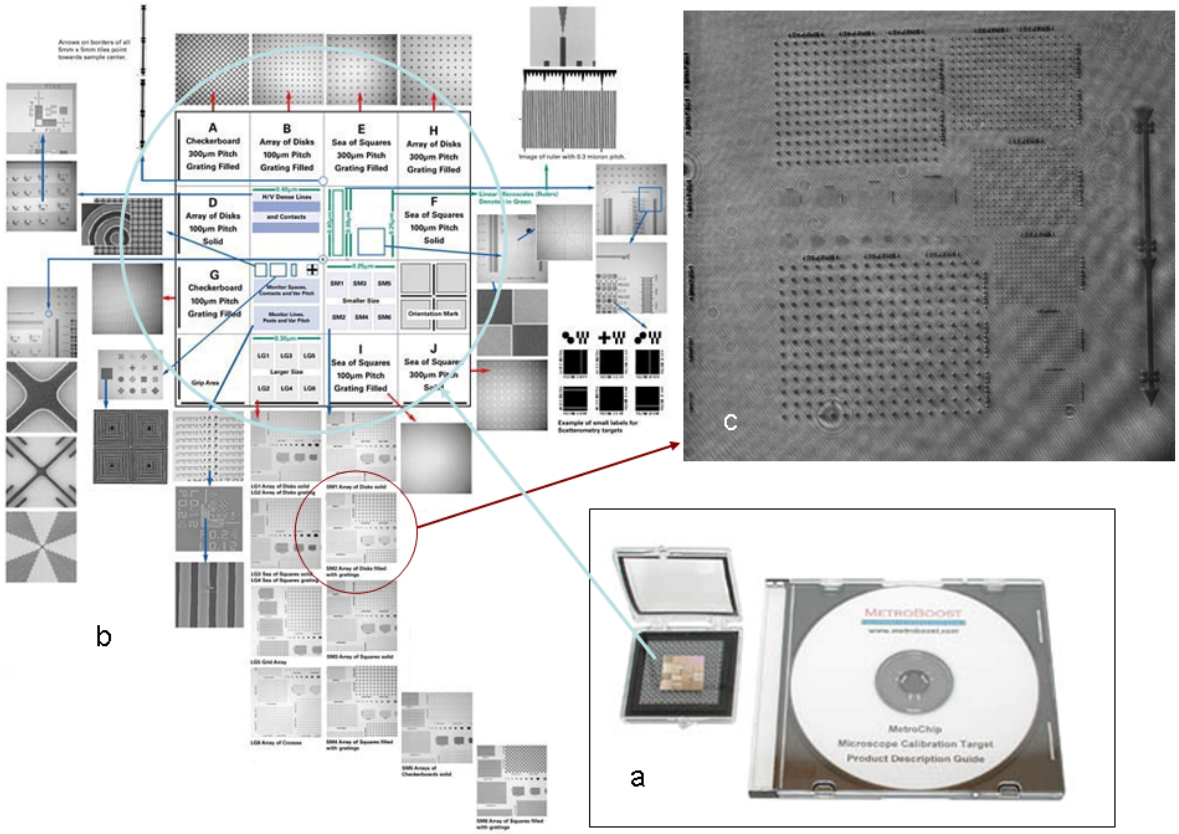

Figure B.1.: a) photo of the Metro Chip b) overview over the structures the chip provides c) picture of a structure taken while adjusting two objective lenses. *Picture Source a) and b): www.tedpella.com*

C. Fourier Transform

The 2-dimensional Fourier transforms reads

$$\mathcal{F}[f(x,y)] = \int f(x,y)e^{-2\pi i(px+qy)}dxdy = F(p,q) \tag{C.1}$$

and the inverse Fourier Transform is

$$\mathcal{F}^{-1}[F(p,q)] = \int F(p,q)e^{2\pi i(px+qy)}dpdq = f(x,y) \tag{C.2}$$

which leads to the unity relation $\mathcal{F}\mathcal{F}^{-1} = 1$.

When (x,y) are spatial coordinates than (p,q) are spatial frequencies and $e^{-2\pi i(px+qy)}$ are plane waves with wavenumber $k = k_x^2 + k_y^2 = \frac{2\pi}{\lambda}$ with $k_x = 2\pi p$, $k_y = 2\pi q$ and the wavelength λ.

This means that a direct Fourier transform resolves a function into a series of plane waves and the original function is written by the superposition of these waves.

Fourier transform theorems Assuming $F(p) = \mathcal{F}[f(x)]$ and $G(p) = \mathcal{F}[g(x)]$, then the following theorems are valid

- similarity theorem: $\mathcal{F}[f(ax)] = \frac{1}{|a|}F(\frac{p}{a})$
- shift theorem: $\mathcal{F}[f(x-a)] = F(p)e^{-2\pi ipa}$
- Parsval's theorem: $\int |f(x)|^2 dx = \int |F(p)|^2 dp$
- convolution theorem: $\mathcal{F}[f(x) \otimes g(x)] = \mathcal{F}[\int f(u)g(x-u)du] = F(p)G(p)$
- autocorrelation theorem: $\mathcal{F}[|f(x)|^2] = \int F(u)F^*(u-p)du$
  or $\mathcal{F}[\int f(u)f^*(u-x)du] = |F(p)|^2$

Note: The similarly theorem means that a broadening of the x coordinate in space leads to a contraction of the coordinate p in the frequency space. The shift theorem means that a translation of the function in space leads to a linear phase shift in the Fourier space. The Parsval's theorem is a expression of energy conversation. In the special case of $g(x) = f^*(-x)$ the autocorrelation theorem evolves into the convolution theorem.

D. Zemax Data

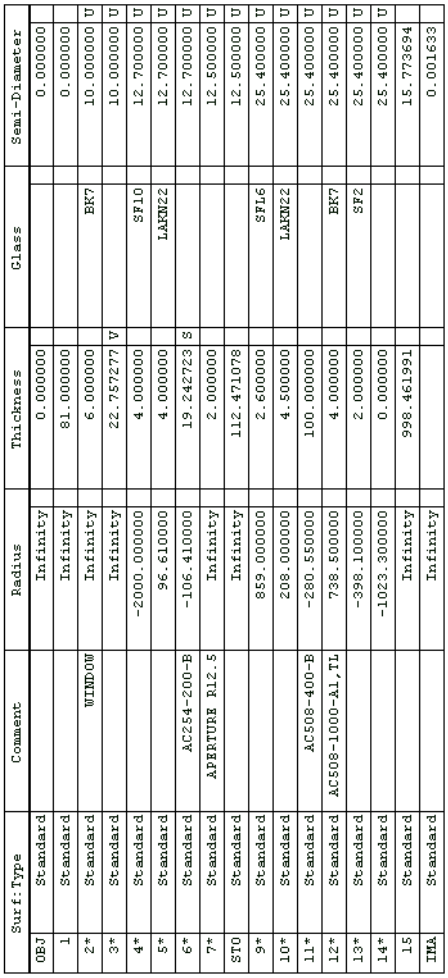

	Surf:Type	Comment	Radius	Thickness		Glass		Semi-Diameter	
OBJ	Standard		Infinity	0.000000				0.000000	
1	Standard		Infinity	81.000000				0.000000	
2*	Standard	WINDOW	Infinity	6.000000		BK7		10.000000	U
3*	Standard		Infinity	22.757277	V			10.000000	U
4*	Standard		-2000.000000	4.000000		SF10		12.700000	U
5*	Standard		96.610000	4.000000		LAKN22		12.700000	U
6*	Standard	AC254-200-B	-106.410000	19.242723	S			12.700000	U
7*	Standard	APERTURE R12.5	Infinity	2.000000				12.500000	U
STO	Standard		Infinity	112.471078				12.500000	U
9*	Standard		859.000000	2.600000		SF16		25.400000	U
10*	Standard		208.000000	4.500000		LAKN22		25.400000	U
11*	Standard	AC508-400-B	-280.550000	100.000000				25.400000	U
12*	Standard	AC508-1000-A1,TL	738.500000	4.000000		BK7		25.400000	U
13*	Standard		-398.100000	2.000000		SF2		25.400000	U
14*	Standard		-1023.300000	0.000000				25.400000	U
15	Standard		Infinity	998.461991				15.773694	
IMA	Standard		Infinity					0.001633	

Figure D.1.: Andor Lens Data

	Surf:Type	Comment	Radius	Thickness		Glass		Semi-Diameter	
OBJ	Standard		Infinity	0.000000				0.000000	
1	Standard		Infinity	81.000000				0.000000	
2*	Standard	WINDOW	Infinity	6.000000		BK7		10.000000	U
3*	Standard		Infinity	22.757277	V			10.000000	U
4*	Standard		-2000.000000	4.000000		SF10		12.700000	U
5*	Standard		96.610000	4.000000		LAKN22		12.700000	U
6*	Standard	AC254-200-B	-106.410000	19.242723	S			12.700000	U
7*	Standard	APERTURE R12.5	Infinity	2.000000				12.500000	U
STO	Standard		Infinity	112.471078				12.500000	U
9*	Standard		859.000000	2.600000		SF16		25.400000	U
10*	Standard		208.000000	4.500000		LAKN22		25.400000	U
11*	Standard	AC508-400-B	-280.550000	100.000000				25.400000	U
12*	Standard	AC508-1000-A1,TL	738.500000	4.000000		BK7		25.400000	U
13*	Standard		-398.100000	2.000000		SF2		25.400000	U
14*	Standard		-1023.300000	400.000000				25.400000	U
15	Standard	F175	100.668000	3.000000		N-BK7		9.446824	
16	Standard		-81.886000	2.500000		N-SF5		9.361427	
17	Standard		-286.880000	135.732000				9.280129	
IMA	Standard		Infinity					0.002800	

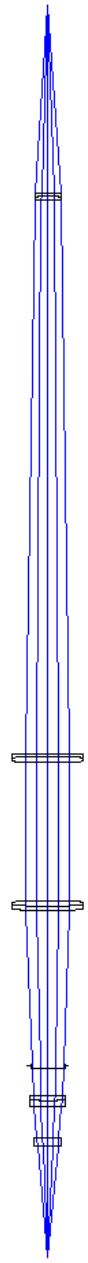

Figure D.2.: Pixelfly Lens Data and Layout

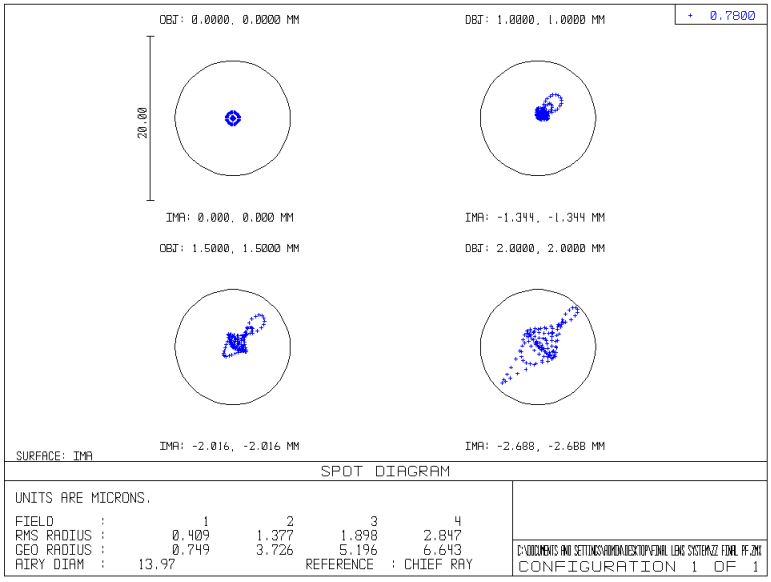

Figure D.3.: Pixelfly Spot Diagram

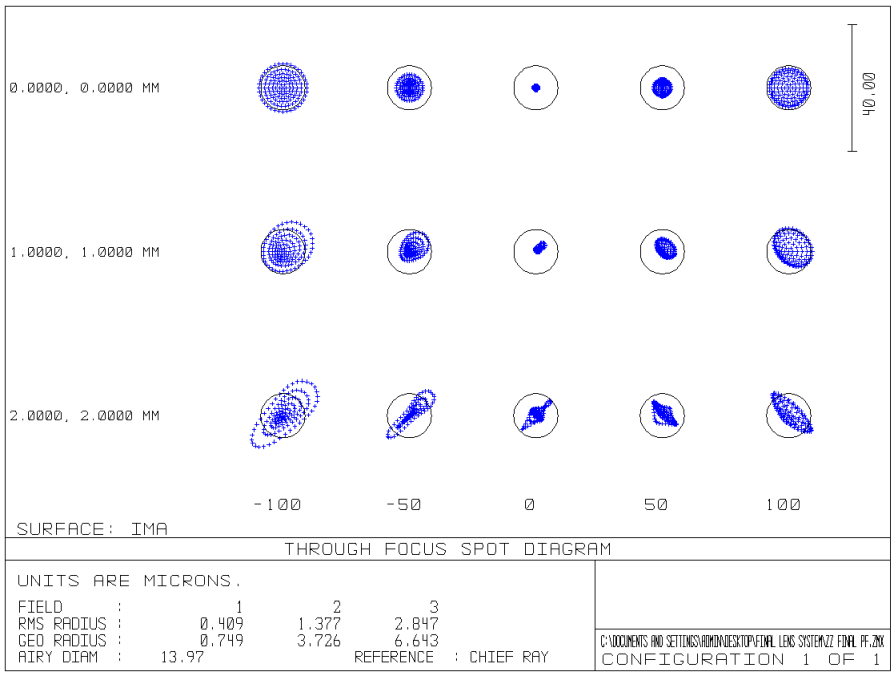

Figure D.4.: Pixelfly Through Focus Spot Diagram

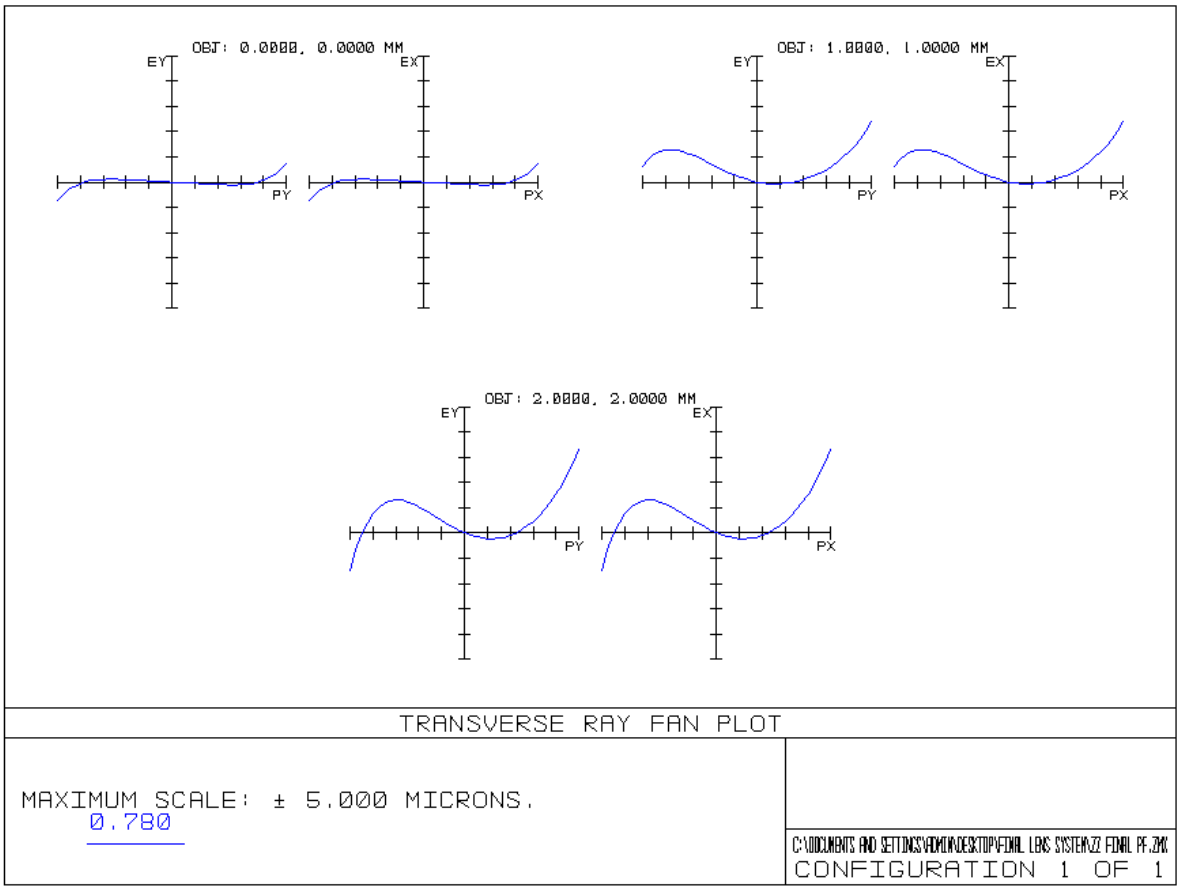

Figure D.5.: Pixelfly Ray Fan

E. Drawings

On the next pages you find construction drawings of two self-made elements within the imaging setup.

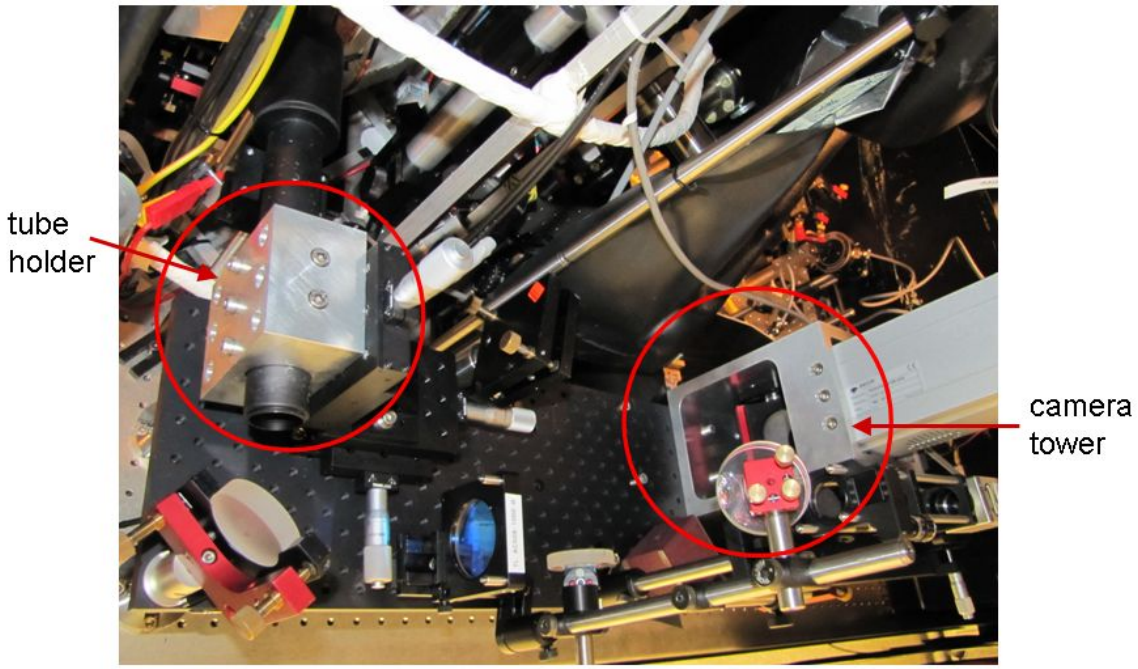

Figure E.1.: Photograph of the setup and the self-made components.

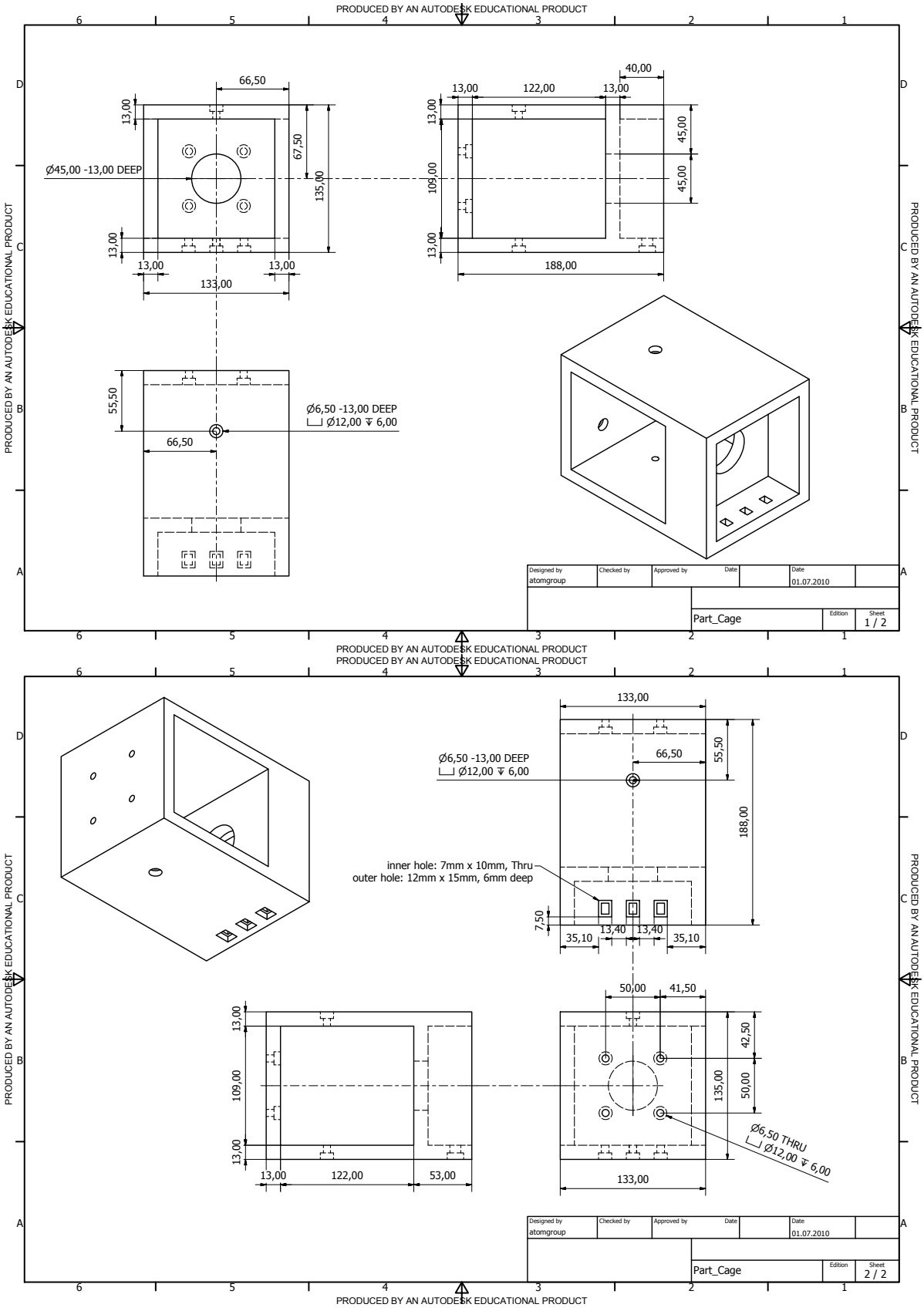

Figure E.2.: Tower for camera mounting

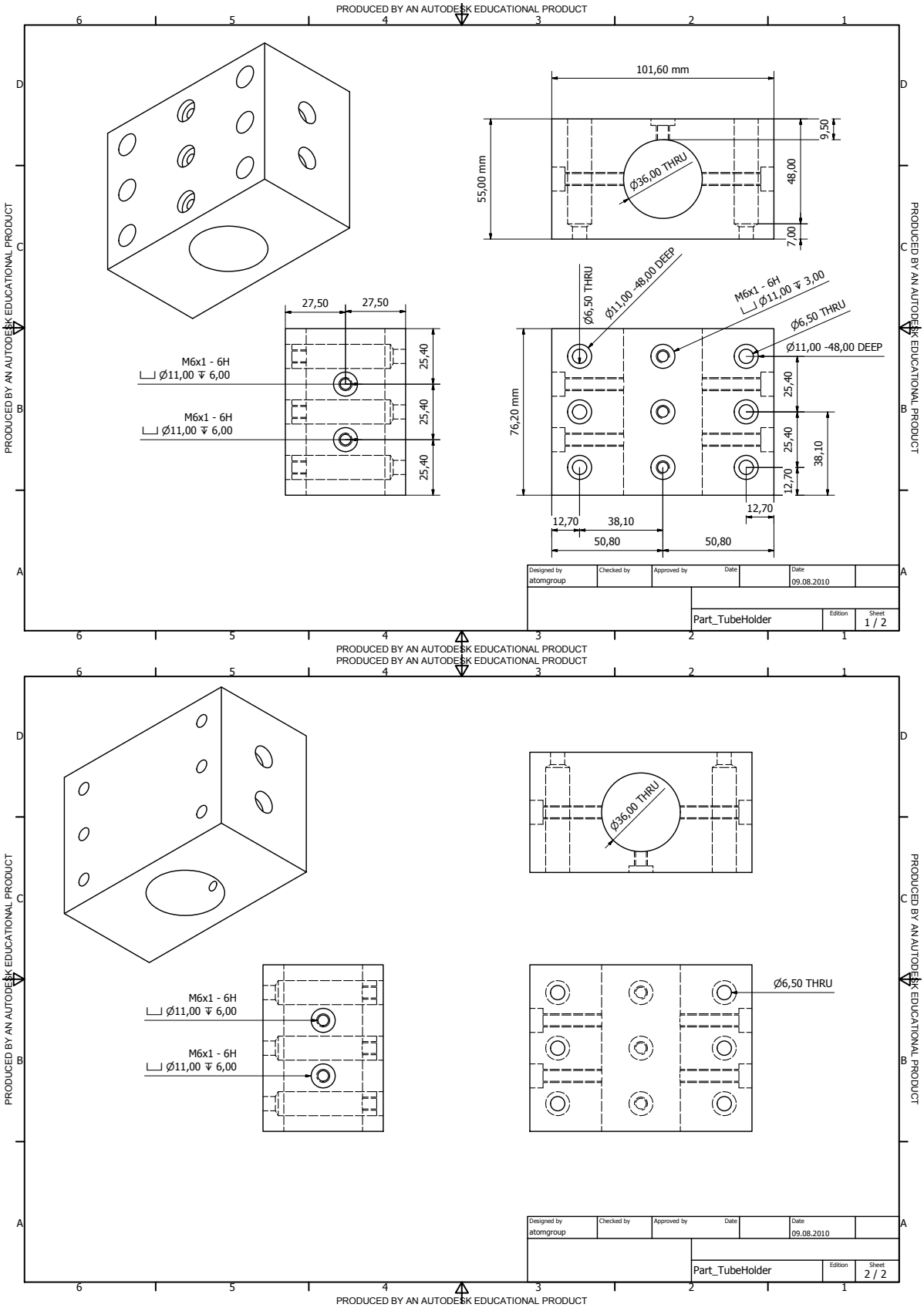

Figure E.3.: Tube holder for objective mounting

Once we accept our limits,
we go beyond them.

Albert Einstein